Russian Chemical Reviews **77** (7) 583 – 600 (2008) © 2008 Russian Academy of Sciences and Turpion Ltd

DOI 10.1070/RC2008v077n07ABEH003775

Hydrophobic materials and coatings: principles of design, properties and applications

L B Boinovich, A M Emelyanenko

Contents

I.	Introduction	583
II.	Factors responsible for wetting of material surface	583
III.	Highly hydrophobic state of material surface and wetting hysteresis	587
IV.	Methods of preparation of textured superhydrophobic surfaces	591
V.	Coating of smooth and textured surfaces with hydrophobic agents	594
VI.	Ageing and degradation of superhydrophobic coatings	595
VII.	Applications of highly hydrophobic and superhydrophobic materials and coatings	597
VIII.	Conclusion	599

Abstract. Theoretical grounds of the design of hydrophobic materials and coatings and the specific features of the superhydrophobic state of the surface are discussed. The possibilities of the formation of various types of ordered textures that ensure high contact angles on the surfaces of hydrophobic materials and prerequisites for thermodynamic stability of the heterogeneous wetting regime of such surfaces are analysed. The main groups of methods actively used now to design materials and coatings with specified topology and structure and variable hydrophobicity are presented. The problems of ageing and degradation of superhydrophobic coatings are discussed. Examples of successful use of superhydrophobic materials in various fields of industry are given. The bibliography includes 111 references.

I. Introduction

Traditionally, by hydrophobic materials are meant materials and coatings for which the contact angle of water and aqueous solutions is larger than 90°. A feature of such materials is instabilty of thin wetting water layers on their surfaces. Hydrophobicity is the property that is determined by the properties and structure of the near-surface layer a few nanometres thick rather than by the characteristics of the bulk material. Therefore, the design of hydrophobic materials and coatings first of all requires analysis of the processes occurring in nanoscale systems, which is a typical problem in nanotechnology.

Practically interesting highly hydrophobic materials are characterised by the water advancing contact angles exceeding 120°. Among them, a particular place is occupied by superhydrophobic materials and coatings characterised by large contact angles ($>150°$) and small slope angles of the surfaces and horizon at which water droplets slide from the surface.

Hydrophobic and superhydrophobic materials possess a set of unique functional properties, namely, they are waterproof, corrosion-resistant and stable against biofouling and inorganic and (in some cases) organic pollutants. The fluid flow near hydrophobic surfaces of such materials occurs with particular ease. Owing to the variety of functional properties, the design of hydrophobic materials and coatings has become an individual avenue of modern materials science, which has been rapidly developing in the Russian Federation and abroad. This is accompanied by an increase in the number of publications concerning specific features of wetting of superhydrophobic surfaces, description of new methods of preparation of textured surfaces, design of novel hydrophobic agents, formation of conditions and compositions for the preparation of surfaces with switchable wetting.

In this review, we will briefly outline the fundamentals of the design of hydrophobic and superhydrophobic materials and coatings, the effect of the chemical structure and specific features of topography on the attainable values of the contact and sliding angles of liquid drops on the surfaces of such materials. We will also dwell on the most interesting methods of the design of materials and nanocoatings with specified topology, structure and variable hydrophobicity. Data on ageing and degradation of superhydrophobic coatings will be briefly analysed in a separate Section. The most successful fields of application of such materials are also discussed.

II. Factors responsible for wetting of material surface

Thomas Young [1] was the first who considered and described the forces acting on a liquid drop more than two centuries ago. He considered an ideal (chemically inert towards the test liquid), smooth and homogeneous surface (Fig. 1 *a*,*b*). It was shown that the equilibrium macroscopic contact angle θ_0

L B Boinovich, A M Emelyanenko A N Frumkin Institute of Physical Chemistry and Electrochemistry, Russian Academy of Sciences, Leninsky prosp. 31, 119991 Moscow, Russian Federation. Fax (7-495) 955 44 43, tel. (7-495) 955 46 25, e-mail: boinovich@mail.ru (L B Boinovich), ame@phyche.ac.ru (A M Emelyanenko)

Received 21 December 2007
Uspekhi Khimii **77** (7) 619 – 638 (2008); translated by A M Raevskiy

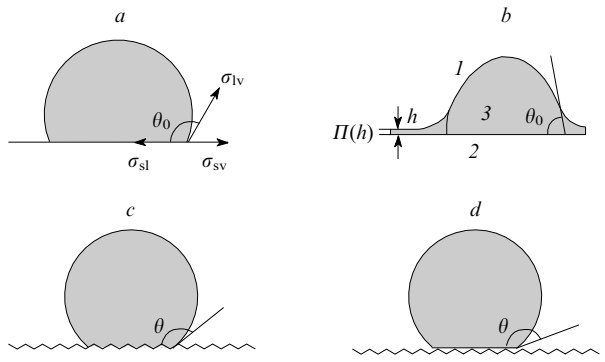


Figure 1. A droplet on a substrate.
Smooth hydrophobic substrate (*a*), smooth hydrophilic substrate (*b*), homogeneous wetting on a rough substrate (*c*) and heterogeneous wetting on a rough substrate (*d*). For notations *1–3*, see text; θ is the effective contact angle.

between the meniscus of the bulk liquid and the substrate is given by

$$\cos\theta_0 = \frac{\sigma_{sv} - \sigma_{sl}}{\sigma_{lv}}, \qquad (1)$$

where σ_{sv} and σ_{sl} are the surface energies at the solid/vapour and solid/liquid interfaces, respectively, and σ_{lv} is the surface tension of the liquid. Generally, σ_{sv} differs from the surface energy at the solid/vacuum interface because the solid surface is covered with a thin wetting/adsorption film of the liquid that is in equilibrium with the liquid drop and vapour. Analysis of Young's relation (1) showed that hydrophobicity can only be observed on solid surfaces with low σ_{sv}.

As σ_{sv} decreases, the contact angle increases. As an illustration, Table 1 lists the surface energies and the contact angles on smooth surfaces of some materials. The following should be emphasised: the free energy of a surface is determined by surface forces that rapidly fade towards the interior of the bulk phase;[6] therefore, hydrophobic properties can be imparted to the surface by coating a high-energy surface with a nanometre-thick layer of an appropriate material. For instance, in Fig. 2 the water contact angles and the surface energy of a gold substrate covered with a self-assembled monolayer made of $HS(CH_2)_{15}COOH$ and $HS(CH_2)_{17}CH_3$ molecules are plotted *vs.* concentration of $HS(CH_2)_{15}COOH$. Coating with a monolayer of $HS(CH_2)_{17}CH_3$ molecules is

Table 1. Surface energies of solids and water advancing angles on smooth surfaces of some materials.

Material	Surface energy /mJ m^{-2}	Contact angle /deg	Ref.
Poly(methylpropenoxy-fluoroalkylsiloxane) with the number of CF_2 groups (n)			
$n = 3$	14.2	105	2
$n = 5$	16.4	102.4	2
$n = 7$	12.6	106.7	2
$n = 9$	12.2	109.3	2
Poly(tetrafluoroethylene)	21	110	2, 3
Octadecanethiol	20	117	4
Perfluoroeicosane	6.7	122	5

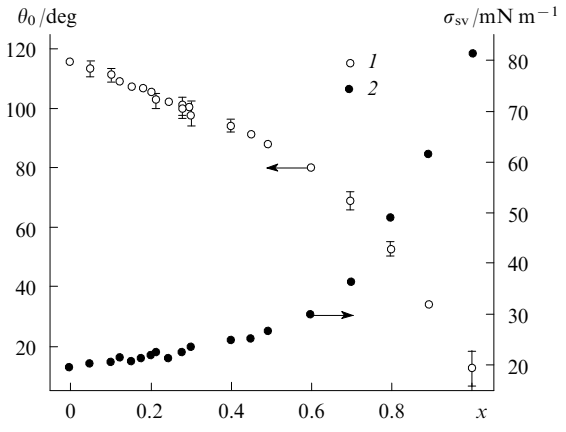


Figure 2. Water contact angle (*1*) and the surface energy (*2*) of a gold substrate covered with a self-assembled monolayer made of $HS(CH_2)_{15}COOH$ and $HS(CH_2)_{17}CH_3$ molecules plotted *vs.* concentration of $HS(CH_2)_{15}COOH$ (x).[4]

sufficient to make the surface hydrophobic. Below (see Section V) we will show that not only the chemical composition of the coating, but also the coating procedure determining the degree of ordering and orientations of surface molecules strongly affect the wettability of materials.

Another approach to the description of wetting of smooth homogeneous surfaces was proposed by Derjaguin and Frumkin. They developed a theory of wetting,[6] which makes it possible to relate the macroscopic contact angle θ_0 (see Fig. 1 *b*) to the disjoining pressure isotherm $\Pi(h)$, which characterises the dependence of the forces of the interaction between phases *1* and *2*, which confine the wetting/adsorption film of liquid *3*, on the film thickness h

$$\cos\theta_0 = 1 + \frac{1}{\sigma_{lv}}\Pi(h_e)\, h_e + \frac{1}{\sigma_{lv}}\int_{h_e}^{\infty}\Pi(h)\mathrm{d}h \approx \qquad (2)$$

$$\approx 1 + \frac{1}{\sigma_{lv}}\int_{h_e}^{\infty}\Pi(h)\mathrm{d}h,$$

where h_e is the equilibrium thickness of the wetting film at the disjoining pressure equal to the capillary pressure in the drop. The radii of curvature of the meniscus and drops used for experimental measurements of contact angles usually lie between 1 and 20 mm, which corresponds to the capillary and disjoining pressures of at most 1 mPa. In this case, the h_e value is almost equal to the film thickness h_0 corresponding to the zero-disjoining-pressure point in the isotherm (Fig. 3).

Specific features of the three-phase equilibrium were analysed in numerous studies (see, *e.g.*, Refs 6–8). It was shown that wetting depends on the shape of the disjoining pressure isotherms (see Fig. 3), which in turn are determined by the nature of surface forces acting in the system under study.[9] In particular, for type *1* isotherms the integral in Eqn (2) is positive. Such isotherms characterise three-phase systems in which complete wetting with the zero contact angle occurs. In these systems, a liquid droplet placed on a substrate will spread in saturated vapour atmosphere with formation of a macroscopically thick film with the zero contact angle. The *2* and type *3* isotherms correspond to partial wetting.

A basic difference between systems characterised by type *2* and type *3* isotherms is related to specific features of wetting,

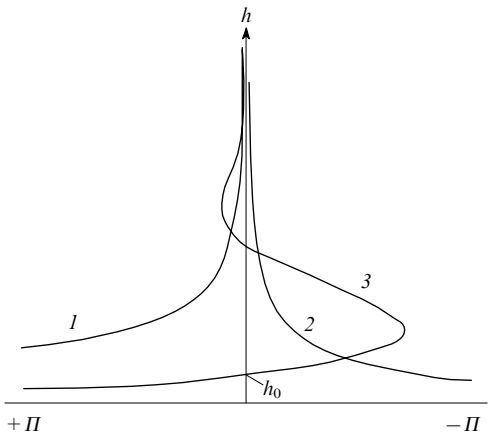


Figure 3. Types of disjoining pressure isotherms. For notations, see text.

which characterise the three-phase equilibrium. In systems with type *2* isotherm a 'sessile' liquid drop is in equilibrium with the 'dry' substrate not covered with liquid molecules, whereas systems with type *3* (S-shaped) disjoining pressure isotherm are characterised by the equilibrium between the drop and the substrate covered with the wetting/adsorption film of finite thickness. In addition, the integral in relation (2) for the systems with type *2* isotherm is always negative; that is why the contact angle differs from zero. The contact angle in the system depends on the ratio of the area under the disjoining pressure isotherm to the surface tension of the liquid. In systems with type *3* isotherm, complete wetting is possible if the integral in expression (2) is positive; otherwise, partial wetting occurs. Formally, large water contact angles on hydrophobic and superhydrophobic surfaces can be attained in systems that are characterised by both type *2* and type *3* isotherms. Here, the action of rather strong attractive (*e.g.*, structural) forces in the system is prerequisite.

Relations (1) and (2) were derived for the equilibrium contact angles, but they can also be used to determine the quasi-equilibrium receding and advancing angles. Here, one should only take into account the thickness difference between the wetting films in expression (2) [and, hence, σ_{sv} in relation (1)] that are in quasi-equilibrium with the receding or advancing fronts of the liquid. Analysis of numerous experimental data on the determination of contact angles on smooth surfaces showed that the hydrophobic properties of the surface layer can be improved only slightly by varying the chemical composition of this layer. Typical values of advancing contact angles on smooth surfaces of bulk materials lie between 100 and 110° (see Refs 3, 10, 11). If a smooth surface is covered with self-assembling monolayers, the advancing contact angles can be as large as 115–116° for dodecanethiol monolayers (see Refs 4 and 12) and 118–120° for monolayers with terminal CF_3 groups (see Refs 5 and 13).

However, smooth homogeneous surfaces are rare in practice; therefore, the applicability of relations (1) and (2) for calculations of contact angles on real surfaces is limited. The effect of the chemical heterogeneity of the surface on the measured contact angle can be included based on the relationship proposed by Cassie [14] (more recently, it was substantiated based on statistical physics treatment [15])

$$\cos\theta = \sum_i f_i \cos\theta_{i0}\,, \tag{3}$$

where f_i is the proportion of the surface area of the ith type of smooth areas on the surface of the material under study, which are characterised by the contact angle θ_{i0}.

Equation (3) can be used if the size of surface inhomogeneities is much smaller than the diameter of the contact area between the liquid drop and the substrate. From Eqn. (3) it follows that contact angle on a smooth heterogeneous surface varies in an interval that is characteristic of each surface type depending on the ratio of the surface areas of fragments of different chemical composition. If a liquid drop is placed on a heterogeneous substrate with a smooth surface with deep pores, two types of equilibrium are possible. One of them occurs if pores are not filled with the liquid (pores in which the liquid contacts the air-vapour phase) while the other occurs when pores are filled with the liquid. Taking into account the fact that in the former case contact angle on the surface of pores (liquid/air-vapour phase interface) is 180°, relation (3) for the smooth surface with unfilled pores is reduced to

$$\cos\theta = f_1(\cos\theta_0 + 1) - 1 \tag{4}$$

(f_1 is the proportion of the surface area occupied by the matrix material), which was first derived by Cassie and Baxter.[16]

In the latter case due to complete wetting ($\theta = 0°$) of the surface of pores filled with the liquid, relation (3) takes the form [17]

$$\cos\theta = f_1(\cos\theta_0 - 1) + 1. \tag{5}$$

The roughness of a wettable surface is the reason for deviation of the measured contact angle from the contact angle on smooth surface. Rough surfaces are characterised by one of the two types of wetting. In homogeneous wetting,[18] the liquid contacts the whole surface of a solid and completely fills all grooves (see Fig. 1 *c*). In heterogeneous wetting,[16] the air (or liquid) is trapped into grooves (see Fig. 1 *d*). For homogeneous wetting the effective contact angle on a rough substrate is calculated using the Wenzel relation [18]

$$\cos\theta = \frac{S}{S_0}\cos\theta_0 = r\cos\theta_0\,, \tag{6}$$

where $r = S/S_0$ is the roughness coefficient equal to the ratio of the actual surface area S to the apparent surface area S_0. Later on, Derjaguin [19] reported a thermodynamic substantiation of this relation for a substrate immersed into a liquid. It was shown that relation (6) holds if the height of spikes on the surface and the distances between them are small compared to the capillary constant of the wetting liquid

$$a = \left(\frac{2\sigma_{lv}}{\Delta\rho g}\right)^{1/2}$$

($\Delta\rho$ is the density difference between the liquid and vapour and g is the acceleration of gravity) and to the radius of curvature of the liquid meniscus in the three-phase contact zone.

From relation (6) it follows that in the case of homogeneous wetting on a rough surface the contact angle increases for hydrophobic surfaces ($\theta_0 > 90°$) and decreases for hydrophilic surfaces ($\theta_0 < 90°$) (Fig. 4).

The second wetting regime occurs on a heterogeneous surface comprised of fragments with the contact angle θ_0 and grooves that are partially or completely filled with air; the effective contact angle is given by the Cassie–Baxter relation [16]

$$\cos\theta = fr\cos\theta_0 + f - 1. \tag{7}$$

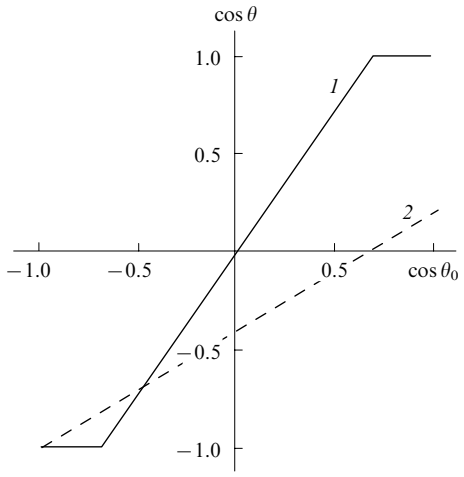


Figure 4. Effective contact angle cosine on a rough substrate plotted *vs.* the Young angle cosine for homogeneous (*1*) and heterogeneous (*2*) wetting.
Calculated for a texture made of square pillars and characterised by a roughness coefficient of 1.4 and a wetted surface area proportion of 0.6.

Here f is the proportion of the projection of the wetted surface area on the substrate surface with inclusion of partial pore filling and r is the roughness coefficient of the wetted surface. Clearly, at $f \to 1$ one deals with transition from heterogeneous to homogeneous wetting of the surface and relation (7) is reduced to expression (6), whereas at $f \to 0$ the wettability of the surface decreases. It should be noted that relationships (6) and (7) can be used to analyse the contact angles of finite liquid drops on substrates only if the characteristic sizes of substrate roughness are much smaller than the diameter of the drop–substrate contact area.

The possibility for a particular wetting regime to occur depends on geometric features of the topography of the solid surface, being somewhat different for the surface contacting a finite drop and the surface immersed into a bulk liquid. Since the superhydrophobic state with heterogeneous wetting seems to be quite promising for some practical applications, we will briefly outline the conditions for occurrence of both wetting regimes.

Theoretical analysis of the conditions for occurrence of the two wetting regimes for a spherical drop on a rough surface was carried out both ignoring gravity and linear tension † (see Refs 20–23) and with partial inclusion of gravity.[24] The parameters corresponding to stable and metastable states of the system in question were determined [20, 21] at different values of the parameters θ and f by minimising the Gibbs free energy. It was shown that the Wenzel regime of homogeneous wetting corresponds to a boundary minimum of the free energy, whereas the Cassie–Baxter heterogeneous wetting corresponds to a local minimum. Heterogeneous wetting on a hydrophobic surface requires that the local minimum of free energy (if exists) be lower than the boundary minimum in the whole range of definition of $f \in 0 \div 1$ and $\theta \in 90 \div 180^\circ$, *i.e.*, be a global minimum. Besides, heterogeneous wetting with partial filling of grooves by the liquid requires meeting an additional condition [20]

$$\frac{\mathrm{d}(rf)}{\mathrm{d}f} = -\frac{1}{\cos\theta_0}, \tag{8}$$

which corresponds to the possibility for the contact angle in the groove to be determined by the Young equation.

Elucidation of a thermodynamically stable wetting regime in the system under study is simplified if one takes into account the fact that the smaller of the two possible contact angles (corresponding to homogeneous or heterogeneous wetting) corresponds to the lower Gibbs free energy and, therefore, to the higher thermodynamic stability.[20–23] As an illustration, we will consider the plot of the cosine of the effective contact angle on a substrate textured with rectangular pillars *vs.* $\cos\theta_0$ (see Fig. 4). Clearly, condition (8) is not met for this topography at $\theta_0 \neq 90^\circ$; therefore, heterogeneous wetting can only occur for those drops that do not penetrate into the inter-pillar space. The contact angles were calculated from relation (6) for homogeneous wetting (solid line) and from expression (5) for heterogeneous wetting (dashed line). According to the results of the analysis, [20–22] the intersection point of the solid and dashed lines corresponds to such a contact angle on the smooth surface (the Young angle) where the contact angles characteristic of the homogeneous and heterogeneous wetting of rough surface are equal to each other. In other words, the two wetting regimes are characterised by the same free energy and therefore each of them can occur equiprobably. Homogeneous wetting is thermodynamically more stable for smaller Young angles, while heterogeneous wetting is more preferable for larger Young angles.

If the surface of a system has a complex topography, the Gibbs free energy of the system can have several local minima in the range of definition of θ and f separated by energy barriers.[22, 25] Such systems can exist in metastable states, the transitions to more stable states at low barriers being spontaneous. If the potential barrier is high enough, the transition from metastable heterogeneous to stable homogeneous wetting can be induced by vibration or be a result of the pressure of the drop against the substrate or due to the kinetic energy of the falling drop.[23, 26–29]

It is noteworthy that the angles θ for metastable states can differ from the corresponding angles for stable states by tens of degrees; this is apparent attainment of superhydrophobic state. Moreover, from relation (7) it follows that the existence of hydrophobic (oleophobic) metastable states associated with air trapping in a rough structure is possible even on hydrophilic (oleophilic) textured surfaces,‡ which was actually observed in the experiments.[30–33] However, such a pseudohydrophobicity is metastable and can hardly be used in practice owing to transition to stable homogeneous wetting regime with the angle $\theta < \theta_0 < 90^\circ$ under the action of external factors. The reverse transition from metastable homogeneous to stable heterogeneous wetting was also observed in the systems where the primary droplet was formed by condensation of strongly supersaturated vapour onto a cooled hydrophobic substrate textured with pillars.[34–36]

† Linear tension characterises the excess energy per unit length of the three-phase contact line. Rigorous treatment of the equilibrium requires taking account of the contribution of linear tension to the total free energy of the system. Analysis and evaluation of this contribution are particularly important when considering equilibria in those systems where the three-phase contact line has a small radius of curvature.

‡ One of the referees kindly attracted our attention to the fact that it is the apparent hydrophobicity of porous hydrophilic surface that is responsible for poor wetting of sand and dust with first drops of rain.

Now we will consider conditions for transition from heterogeneous to homogeneous wetting for a rough surface immersed into a bulk liquid. Similar problems arise in the design of materials for, *e.g.*, underwater structures, ship hulls, *etc*. Thermodynamic consideration of the conditions for stability of different wetting regimes on underwater surfaces has some specific features. On the one hand, there is no need of inclusion of the changes in the energy of the free surface of the drop due to the change in the shape of the drop upon the change in the wetting regime. On the other hand, one should take into account the change in the potential energy of the system as the air bubbles trapped in the grooves on the surface are replaced by the liquid.

Changes in the free energy of a system comprised of a rough substrate immersed into a liquid on going from homogeneous to heterogeneous wetting in a single groove are given by

$$\Delta G = \sigma_{sv} S_2 + \sigma_{lv} S_1 - \sigma_{sl} S_2 + \Delta\rho g H V = \quad (9)$$

$$= (S_2 \cos\theta_0 + S_1)\sigma_{lv} + \Delta\rho g H V,$$

where S_1 and S_2 are the areas of the liquid/gas interface and the unwetted surface of the groove, respectively (Fig. 5), and H and V are respectively the depth of immersion and the groove volume (it is assumed that the size of the gas bubble is much smaller than the depth of immersion).

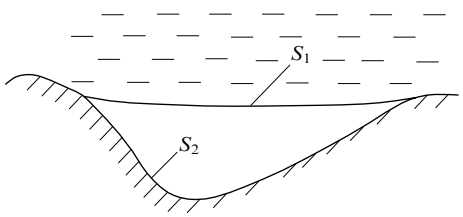


Figure 5. An illustration for calculations of changes in the free energy on going from homogeneous to heterogeneous wetting in a single groove of a rough substrate on dipping into the liquid.

Heterogeneous wetting is thermodynamically stable at negative ΔG. A positive change in the free energy in the transition in question corresponds to homogeneous wetting, *i.e.*, to filling of grooves with the liquid. If the last term in Eqn (9) is small compared to the first term, one gets a simple but very important expression for the choice of the surface topography necessary to ensure heterogeneous wetting, namely

$$\frac{S_2}{S_1} > -\frac{1}{\cos\theta_0}. \quad (10)$$

Taking into account the fact that the Young angle is usually at most 120°, we obtain that stable heterogeneous wetting can occur only in those systems where the unwetted surface area of the groove *a priori* exceeds the doubled surface area of the liquid/gas interface. This makes the topography with grooves extending towards the bottom more preferable. On the contrary, if the height of spikes on the surface is much smaller than the spike–spike separation, homogeneous wetting will occur. However, it should be remembered that here, as in the case of a drop on the surface, the position of the liquid/gas interface in the groove should meet the condition (8).[37]

The requirements for surface topography to ensure heterogeneous wetting of a substrate on deep immersion are specified by Eqn (9); they are much more rigorous (due to the last term) than those specified by inequality (10); however, the effect of the term mentioned above becomes negligible for micrometre-size grooves.

III. Highly hydrophobic state of material surface and wetting hysteresis

In the preceding Section, we noted that by varying the chemical composition of a material or using various hydrophobising agents, one cannot achieve the contact angles larger than 120° on smooth surfaces. To prepare materials with larger contact angles, one should use the combined effect of the surface roughness and chemical structure. It is 'tuning' of the surface texture that allows superhydrophobic states to be attained. Most modern methods make it possible to prepare highly hydrophobic materials based on disordered surface textures (see Section IV). In this case, process conditions for surface coating or treatment are chosen in the course of lengthy and laborious experiments. At the same time, such methods, as, *e.g.*, coating from dispersions, photolithographic and template techniques permit preparation of highly ordered and well controllable surface roughness. Here we will analyse the effect of parameters of ordered textures on the contact angle and wetting hysteresis in more detail.

The simplest example to be analysed is a texture based on pillars or holes that obey an ordered pattern on the surface of a material. Depending on the method of texturing and template used,[13, 23, 25, 26, 34–40] various shapes of cross-sections of these structures can be obtained. By varying the height, size and distance between the elements of the texture one can vary the surface roughness and contact angle over a wide range. As an example, Table 2 lists the data taken from Ref. 38 in which the surface was textured with square pillars of size $a = 50$ μm separated by the distance $b = 100$ μm. By varying the height c, one can both vary the contact angle in the Wenzel regime over a wide range and attain transition to the Cassie–Baxter wetting regime for high roughness determined from the relation

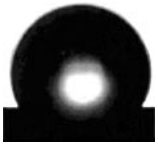
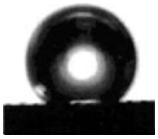
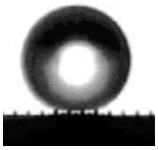
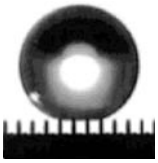
$$r = \frac{(a+b)^2 + 4ac}{(a+b)^2}. \quad (11)$$

The results of measurements of contact angles and calculations based on the Wenzel and Cassie–Baxter relations are in qualitative agreement; quantitative agreement requires the inclusion of a rather high roughness of the pillar surface.

An important feature of the ordered pillar-like surface texture is that the advancing angles can be close to 180°. Additional treatment of the surface of pillars with a hydrophobising reagent causes significant enhancement of the nanostructured roughness and makes it possible to reach the receding angles that are also close to 180° (see Ref. 35).

Yet another type of ordered texture, which is widely used for enhancement of roughness, can be obtained by deposition of spherical particles on the surface. Here, the r value is immediately related to the close-packing coefficient of the particles, the amount of hydrophobising reagent and the presence of fillers in the interparticle space. For instance, if the lower hemispheres of particles are immersed into the matrix (binder or hydrophobising reagent) on the surface treated, the topography is formed by hemispheres or truncated spheres. We have derived relations for calculating the key parameters that characterise wetting of surfaces for different types of close

Table 2. Effect of the height of pillars on the wetting regime and contact angle.

Drop	θ /deg	r	c /μm
	114	1.0	0
	138	1.1	10
	155	1.2	36
	151	2.0	148
	163	3.1	282

packing of monodisperse particles on the surface. For instance, the roughness and the proportion of the wetted surface area for square packing of spherical particles and hemispheres can be calculated from the following expressions:
heterogeneous wetting

$$r = \frac{2(1+\cos\theta_0)}{\sin^2\theta_0}, \tag{12a}$$

$$f = \frac{\pi}{4}\sin^2\theta_0; \tag{12b}$$

homogeneous wetting ($f = 1$)
for hemispheres

$$r = 1 + \frac{\pi}{4}, \tag{12c}$$

for spherical particles

$$r = (1+\pi). \tag{12d}$$

The relations for spherical particles were derived assuming that at $\theta_0 > 90^\circ$ the meniscus of the liquid for heterogeneous wetting is above the equator of the particles.

The relations for a hexagonal close packing of both hemispheres and spherical particles have the form:
heterogeneous wetting

$$r = \frac{2(1+\cos\theta_0)}{\sin^2\theta_0}, \tag{13a}$$

$$f = \frac{\pi}{2\sqrt{3}}\sin^2\theta_0; \tag{13b}$$

homogeneous wetting ($f = 1$)
for hemispheres

$$r = 1 + \frac{\pi}{2\sqrt{3}}, \tag{13c}$$

for spherical particles

$$r = 1 + \frac{2\pi}{\sqrt{3}}. \tag{13d}$$

Correspondingly, the contact angles on such textured surfaces for square packing are determined by the following relationships:
heterogeneous wetting

$$\cos\theta = \frac{\pi}{4}\left(1+\cos\theta_0\right)^2 - 1; \tag{14a}$$

homogeneous wetting
for hemispheres

$$\cos\theta = \left(1+\frac{\pi}{4}\right)\cos\theta_0, \tag{14b}$$

for spherical particles

$$\cos\theta = (1+\pi)\cos\theta_0. \tag{14c}$$

The relations for hexagonal packing are as follows:
heterogeneous wetting

$$\cos\theta = \frac{\pi}{2\sqrt{3}}\left(1+\cos\theta_0\right)^2 - 1; \tag{15a}$$

homogeneous wetting
for hemispheres

$$\cos\theta = \left(1+\frac{\pi}{2\sqrt{3}}\right)\cos\theta_0, \tag{15b}$$

for spherical particles

$$\cos\theta = \left(1+\frac{2\pi}{\sqrt{3}}\right)\cos\theta_0. \tag{15c}$$

From expressions (14a–c) and (15a–c) it follows that the radius of spherical particles (hemispheres) has no effect on the contact angles if the surfaces were textured by deposition of monodisperse spherical particles with formation of dense monolayers where adjacent particles contact one another. This conclusion was substantiated experimentally in a study [41] of contact angles on the surface made of hexagonally packed polystyrene beads. It was found that the effective contact angle remained unchanged ($\theta = 131 \pm 2^\circ$) as the diameter of particles varied from 270 to 690 nm. It is noteworthy that the θ value calculated for heterogeneous wetting using relation (15a) and $\theta_0 = 114^\circ$ is 132°.

The contact angles calculated from relations (14a–c) and (15a–c) are plotted in Fig. 6 *vs.* Young angle. From these

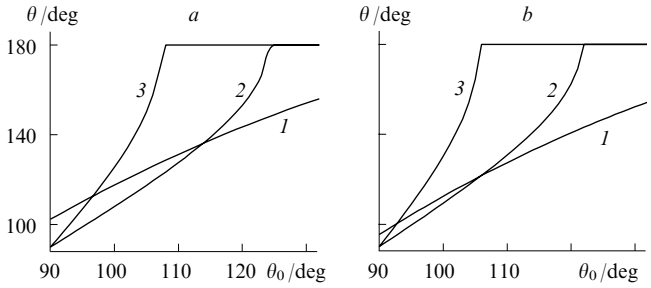


Figure 6. Effective contact angles on a textured surface made of monodisperse spheres for square (*a*) and hexagonal (*b*) close packing plotted *vs.* Young angle [calculated using expressions (14a – c) and (15a – c)]. Heterogeneous wetting (*1*) and homogeneous wetting for spherical particles (*2*) and hemispheres (*3*). The intersection points of lines *1* and *2* (lines *1* and *3* for hemispheres) correspond to the angles of transition from homogeneous to heterogeneous wetting.

data it follows that texturing of weakly hydrophobic surfaces ($\theta_0 < 92^\circ$ for hexagonal close packing and $\theta_0 < 96^\circ$ for square close packing) causes slight increase in the effective contact angle. In this case, homogeneous wetting appears to be thermodynamically more stable. An increase in the Young angle permits transition to heterogeneous wetting at low content of binder or hydrophobising reagent, *i.e.*, where the topography is formed by spherical particles. In this case, the square close packing ensures larger effective contact angles. At the same time, if coating of a substrate was accompanied by embedding of the particles into the polymer matrix (binder and/or hydrophobising reagent) and the topography is determined by truncated spheres, the wetting will be governed by the Wenzel law as in the case of small Young angles.

Thus, comparison of the data in Figs 6 *a* and *b* shows that the highest hydrophobicity on dense texturing using monodisperse particles is attained for a looser square packing and shallow immersion of particles into the polymeric matrix. However, one should keep in mind that such a texture is less stable to mechanical action. Finally, an important result is the fact that a superhydrophobic surface cannot be prepared at close packings of monodisperse particles irrespective of particle size.

In loosely packed systems, a new degree of freedom appears. For instance, the contact angles on the surface for loose hexagonal packing are given by:
heterogeneous wetting

$$\cos\theta = \frac{2\pi}{\sqrt{3}}\left(\frac{R}{D}\right)^2\left(1+\cos\theta_0\right)^2 - 1; \tag{16a}$$

homogeneous wetting
for hemispheres

$$\cos\theta = \left[1+\frac{2\pi}{\sqrt{3}}\left(\frac{R}{D}\right)^2\right]\cos\theta_0\,, \tag{16b}$$

for spherical particles

$$\cos\theta = \left[1+\frac{8\pi}{\sqrt{3}}\left(\frac{R}{D}\right)^2\right]\cos\theta_0\,, \tag{16c}$$

where R is the radius of the spherical particle and D is the distance between the centres of adjacent spheres in the lattice.

From relations (16a – c) it follows that a decrease in the R/D ratio causes an increase in the effective contact angle in the system for heterogeneous wetting and a decrease in this angle for homogeneous wetting. However, it is the wetting regime corresponding to the smaller of the two contact angles that will be thermodynamically more stable (see above). Analysis of expressions (16a – c) showed that an increase in the distance between the centres of spherical particles will cause the effective contact angle corresponding to the equilibrium state to increase initially (heterogeneous wetting), reach a maximum value (at equal probability of the homogeneous and heterogeneous wetting regimes) and then decrease (homogeneous wetting). Clearly, it is important to determine the $(R/D)_t$ ratio corresponding to transition from heterogeneous to homogeneous wetting at a fixed Young angle. From relations (16a – c) for a hexagonal texture made of spherical particles, we get

$$\left(\frac{R}{D}\right)_t = \frac{1}{1-\cos\theta_0}\left[\frac{\sqrt{3}(1+\cos\theta_0)}{2\pi}\right]^{1/2}. \tag{17}$$

Substituting the $(R/D)_t$ ratio calculated using expression (17) into relations (16a – c), we obtain the angle characterising the maximum attainable (by choosing the R/D ratio) hydrophobicity of the surface with the Young angle θ_0 (Fig. 7). According to the calculations, the superhydrophobic state on a textured surface formed by monodisperse particles can be reached using two scaling factors associated with the particle size and interparticle distance. However, the requirements imposed in this case on the Young angle ($\theta_0 > 113$ °C) and on the inter-particle distance ($R/D < 0.3$) are quite rigorous and therefore the desired surface textures are prepared using special technological procedures.

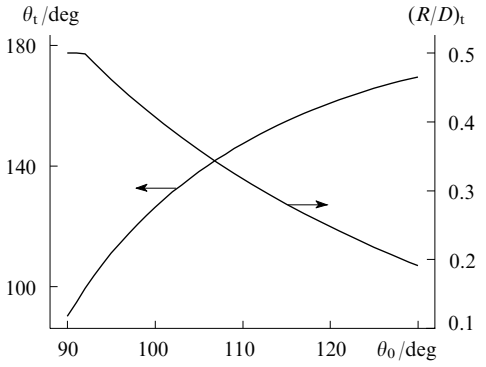


Figure 7. R/D_t ratio calculated using Eqn (17) and effective contact angle θ_t corresponding to wetting transition plotted *vs.* Young contact angle.

Another situation occurs in the case of particle aggregation on the surface with formation of multimodal roughness.[12,42–45] In the simplest case this is a bimodal texture prepared using two types of particles of strongly different size, namely, the surface is coated with large particles covered with a monolayer of small particles. As the roughness coefficient significantly increases for close packings, in this texture, on the one hand, homogeneous wetting becomes thermodynamically unfavourable even on weakly hydrophobic particles and, on the other hand, the proportion of the wetted surface area decreases, which in turn leads to an increase in the contact angle for heterogeneous wetting. It should be emphasised that

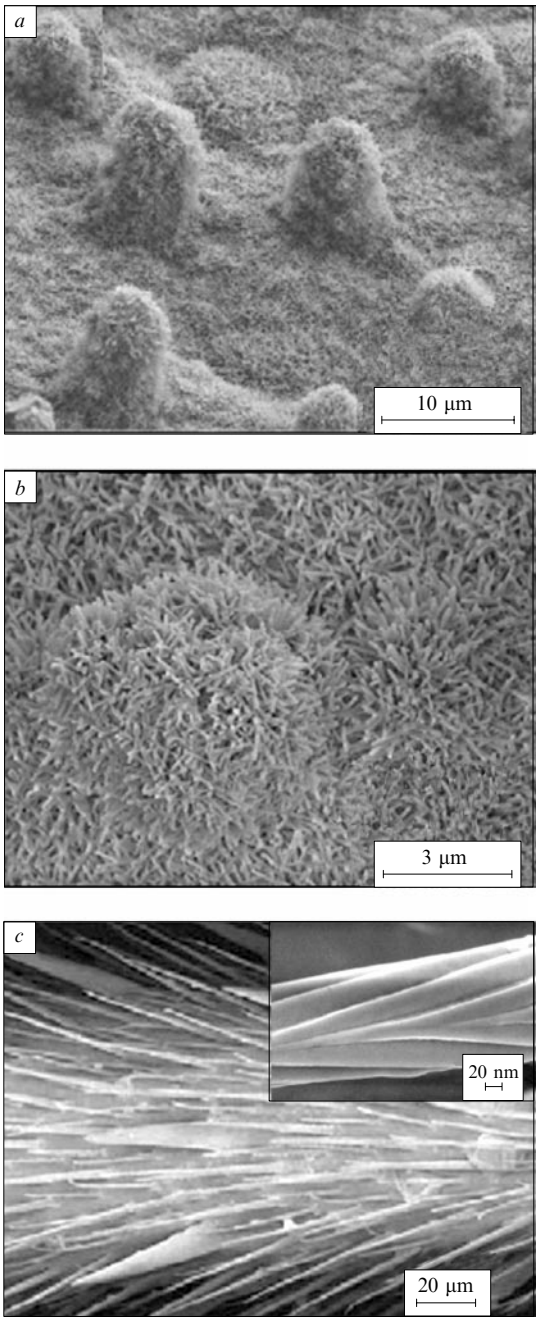


Figure 8. Surface textures: the leaf of lotus *Nelumbo nucifeara* at different magnification (*a*, *b*) [46] and the legs of water strider *Gerris hemigis* (*c*).[31]

almost all superhydrophobic surfaces based on both artificial disordered textures and textured natural materials (Fig. 8) are characterised by multimodal roughness.

Up to this point we have discussed the effect of specific features of textures on the contact angle. However, the most attractive for practical use are those superhydrophobic materials that are characterised by not only large advancing contact angles, but also small sliding angles, α, of liquid drops (see Introduction). It is the small value of the angle α that unambiguously points to predominance of heterogeneous wetting where the surface area of the substrate–water contact is minimal. The angle α is first of all determined by the mass of the drop and by the contact angle hysteresis defined as the difference between the advancing angle (θ_{adv}) and the receding angle (θ_{rec})

$$\Delta\theta = \theta_{adv} - \theta_{rec} ,$$

therefore we will dwell on the effect of surface texture on $\Delta\theta$.

In their fundamental study, Dettre and Johnson [47] systematically investigated the effect of roughness on the receding and advancing angles (Fig. 9). The experimentally observed hysteresis of the contact angle for the surfaces coated with fluorocarbon and paraffin waxes was 15° and 8°, respectively. Initially, as the roughness of both surfaces increased, the advancing angle increased and the receding angle decreased. As a result, the hysteresis increased to 100° on fluorocarbon waxes and to 85° on paraffin waxes. In the second step, upon attainment of a certain critical roughness, the receding angle behaves in different manner, namely, an increase in roughness was accompanied by fast increase in the receding angle and simultaneous much slower increase in the advancing angle. Finally, the third step was characterised by almost constant value of the advancing angle and a slight increase in the receding angle. As a result, the contact angle hysteresis is much smaller than for smooth surfaces and corresponds to sliding angles of a few degrees.

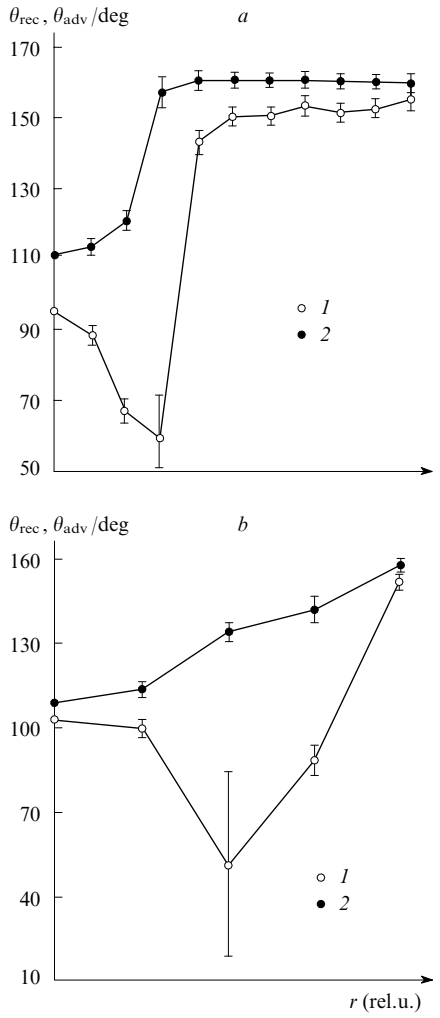


Figure 9. Effect of roughness on the receding angle (*1*) and advancing angle (*2*) on the surface covered with fluorocarbon (*a*) and paraffin (*b*) waxes.

This pattern of changes in the contact angle hysteresis with an increase in roughness was observed in numerous more recent studies. It is associated with manifestation of homogeneous wetting in the region where the receding angle decreases and heterogeneous wetting in the region where θ_{rec} rapidly increases. Interestingly, to a first glance the initial decrease in the receding angle from values greater than 90° to those lesser than 90° contradicts the Wenzel relation (6). However, this apparent contradiction can be explained with ease from the standpoint of the Derjaguin – Frumkin theory.

As mentioned above, relations (1) and (2) were derived to describe the equilibrium angles, they can correctly be used for calculations of quasi-equilibrium receding and advancing angles taking into account the actual thicknesses of wetting films that are in equilibrium with the receding and advancing fronts of the liquid. In the case of homogeneous wetting, there is a rough structure with grooves partially filled with the liquid behind the receding front; this leads to an increase in the effective thickness of the wetting film that coexists with the receding drop. Therefore, calculations of the effective receding angle from relation (6) require the use of the receding angle for the drop that is in quasi-equilibrium with the thicker film rather than the receding angle $\theta_{0\,rec}$ on the smooth surface determined for the drop that coexists with the film. According to relation (2), this in turn leads to a decrease in $\theta_{0\,rec}$ for the three-phase systems described by type *2* and type *3* isotherms (see Fig. 3). However, on going to heterogeneous wetting at larger roughness due to the absence of the liquid in grooves, the effective thickness of the liquid film after the receding front rapidly decreases; this causes the angle to increase. Finally, in the case of the limiting attainable receding angles corresponding to the absence of liquid after the receding front the difference between the advancing and receding angles is only determined by the capillary pressure difference between the receding and advancing fronts of the drop. The residual hysteresis depends on the shape of the disjoining pressure isotherm in the region of small negative Π values and is usually very small.

The effect of the mass of the drop (m) on the sliding angle can be estimated as follows. As the tilt angle of the substrate becomes equal to the sliding angle (here the drop is still in equilibrium!), the sum of the projections of the forces acting on the drop along the sliding plane on the inclined plane should be equal to zero. Therefore, the projection of the gravity force, which depends on the tilt angle of the substrate, will be compensated by the sum of wetting tension along the drop – substrate contact line. To a first approximation, in this case one has [3, 48]

$$mg \sin \alpha = \pi R \sigma_{lv} (\cos \theta_{rec} - \cos \theta_{adv}), \quad (18)$$

(R is the radius of the drop – substrate contact), which shows that the sliding angle decreases as the mass of the drop increases and wetting hysteresis decreases.

Thus, it is the small wetting hysteresis associated with wetting transition to heterogeneous wetting, which is responsible for instability of drops on oblique hydrophobic surfaces. Experimental studies of the effect of the mass of the drop on the sliding angle revealed [38] the sliding angle anisotropy on anisotropic textures. The light sliding direction coincided with the direction characterised by continuous drop – substrate contact line (Fig. 10).

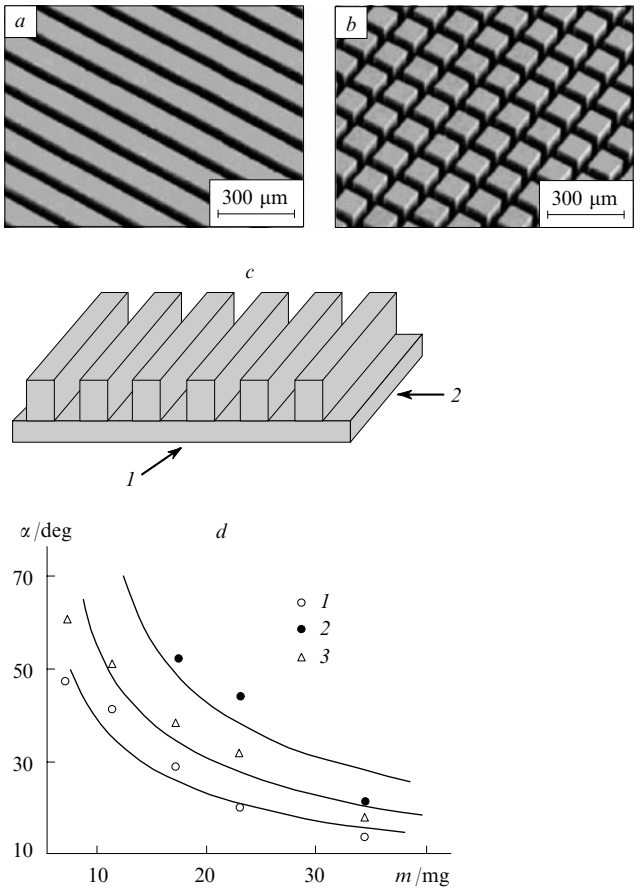


Figure 10. SEM images of the groove structure (*a*) and pillar-like structure (*b*); schematic illustration of the sliding angle measurement direction parallel (*1*) and orthogonal (*2*) to grooves (*c*) and the dependences of the sliding angles on the droplet mass m (*d*).
(*d*): parallel direction (*1*), orthogonal direction (*2*), and pillar-like structure (*3*).[38]

IV. Methods of preparation of textured superhydrophobic surfaces

Systematic research on the design of specific textures suitable for imparting superhydrophobic properties to surfaces of materials began in the 1950s.[47, 49] In the study by Dettre and Johnson [47] (see above), the surface was textured by spraying the substrate with either dispersed paraffin (or fluorocarbon) waxes or heated dispersion of micrometre-size glass beads in a wax solution in hexane. Different roughness was imparted by subsequent fusion of the surface. The effect of surface roughness on the contact angles and on wetting hysteresis was studied systematically.[47]

More recently, a large number of approaches to preparation of textured surfaces necessary to attain the superhydrophobic state of surfaces were proposed. The techniques most widely used at present are as follows:

— coating with thick layers of alkylketene dimers by removal of substrate from melt followed by crystallisation of the coating and formation of a fractal structure;[50, 51]

— solution polymerisation of coatings with the formation of a porous phase on various surfaces;[52, 53]

— chemical vapour deposition of ordered structures followed by treatment with hydrophobic materials;[3, 54 – 58]

— plasma etching of polymer surfaces;[3, 10, 11, 59 – 61]

— coating with films of sublimation materials;[62, 63]

— electrodeposition and electrochemical deposition of nanoparticles and films followed by treatment with hydrophobic materials;[64, 65]

— use of organic and inorganic fillers with multimodal particle size distribution for particles in the matrix of the hydrophobic material;[42–44, 66–71]

— template methods for preparation of rough surfaces with subsequent removal of templates and treatment with hydrophobic materials;[72–76]

— controllable aggregation of nanoparticles on the surface, which leads to multimodal roughness, followed by treatment with hydrophobic materials;[12]

— photolithographic techniques followed by treatment with hydrophobic materials;[13, 23, 25, 26, 39, 40] and

— etching of the surface of materials followed by treatment with hydrophobic materials.[77, 78]

Now we will consider specific features of different techniques in more detail taking some studies cited above as examples.

Plasma-assisted chemical deposition of carbon nanotubes was used for texturing the surface of silicon covered with oxide film.[54] The two main steps of the process include coating of a substrate with a catalyst (in the form of nickel islets) by melting a thin nickel film and growth of carbon nanotubes on the nickel islets in d.c. plasma discharge (acetylene/ammonia gas mixture) at a pressure of 4 mm Hg. Plasma-assisted chemical depositon provides the desired orientation of nanotubes (normal to the substrate). The diameter and number of nanotubes per unit surface area are specified by the size and distribution of the catalyst islets, while the height is proportional to the deposition time. The texture thus prepared exhibits reasonable homogeneity with respect to the distribution of nanotubes over the substrate surface; the shorter the nanotubes the better the homogeneity with respect to height (Fig. 11). However, the contact angles of water droplets on the nanotube textured surfaces lie between 84 and 86°. In particular, it is the fact that the contact angles are smaller than 90° that is responsible for the possibility of water condensation to occur in the space between nanotubes on thermal equilibrium. Here, the capillary effects cause single nanotubes to form bundles,[54] which has a negative effect on the operating properties of nanotubes. Subsequent treatment of the surface of carbon nanotubes also makes use of chemical vapour deposition, namely, thermally activated decomposition of hexafluoropropylene oxide produces CF_2 radicals, which undergo polymerisation and form a thin poly(tetrafluoroethylene) layer on the nanotube surface. Once these procedures completed, the advancing and receding contact angles on the surfaces coated with the 'forest' of hydrophobised nanotubes can be as large as 170 and 160°, respectively.

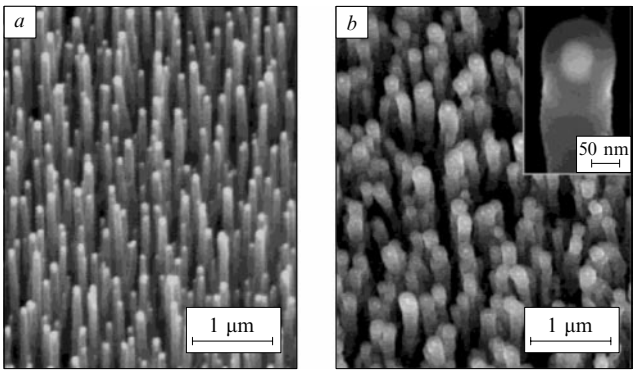


Figure 11. SEM images of a surface covered with carbon nanotubes.[54] Non-hydrophobised surface (*a*) and the hydrophobised surface coated with poly(tetrafluoroethylene) obtained by chemical vapour deposition during thermal decomposition of hexafluoropropylene oxide (*b*).

An interesting example of attainment of the superhydrophobic state by substrates of different nature using plasma etching was reported by Woodward *et al.*[10] A silicon (or potassium bromide) substrate was coated with a polybutadiene film in toluene solution and annealed to remove traces of the solvent. Then the sample was placed in a vacuum chamber (2×10^{-4} atm) filled with carbon tetrafluoride and an electric discharge was switched on. This treatment gave a rough surface of the polybutadiene film, and fluorination of the surface layer occurred simultaneously. The degree of roughness depended on the discharge power (Fig. 12) and on the time of exposure to the discharge. The superhydrophobic state required that the root-mean-square roughness be at least 46.5 nm. The maximum water contact angle on this surface was 175° and wetting hysteresis was at most 1°.

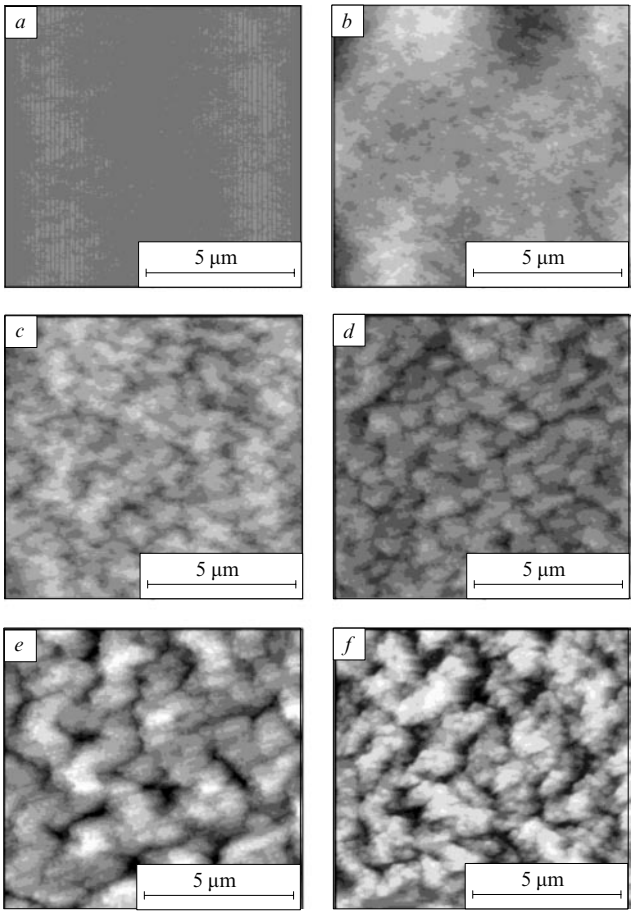


Figure 12. AFM height images of the surface of a polybutadiene film after plasma etching (CF_4 atmosphere, duration = 5 min) at plasma discharge power of 0 (*a*), 10 (*b*), 20 (*c*), 30 (*d*), 40 (*e*), 80 W (*f*).[10]

Coating of the surface of glass with films of sublimation materials containing titania inclusions [62, 63] allowed three practically important problems to be solved at once, namely, to attain the superhydrophobic state, to retain transparency of the coated glass and to perform photocatalytic cleaning of the

surface when operating in air. Figure 13 presents a flow diagram of the process [62, 63] of preparation of similar hydrophobic films based on aluminium hydroxide or silica.

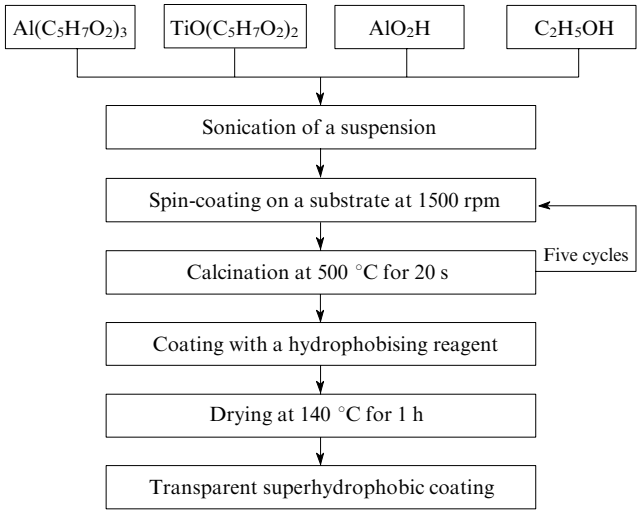
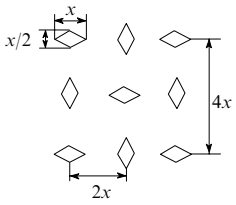
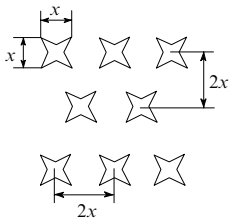
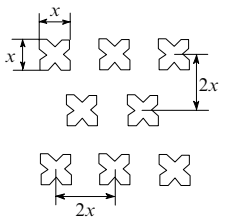
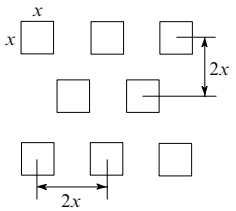


Figure 13. Flow diagram of the processing of titania-containing transparent superhydrophobic coating.[62]

Titanium acetylacetonate, which undergoes thermal decomposition with the formation of titania, is mixed with aluminium hydroxide or silica powder, aluminium acetylacetonate $Al(C_5H_7O_2)_3$ and ethanol to produce a suspension. Sonication of the suspension leads to homogeneous distribution of components and dissolution of $Al(C_5H_7O_2)_3$. The suspension is coated on a glass substrate and dried at room temperature to afford a matt coating. Short-term heat treatment of the coated substrate at 500 °C causes decomposition of titanium acetylacetonate, sublimation of $Al(C_5H_7O_2)_3$ and enhancement of film transparency. The transparency of this system in the visible spectral region strongly depends on both the surface roughness due to sublimation and the content of titania. The coating, drying and calcination of suspension are repeated several times until uniform coating of the substrate is achieved. Hydrophobic properties are imparted to the coating by storing samples in a solution of heptadecafluorodecyltrimethoxysilane in methanol at room temperature for 1 h and subsequent drying at 140 °C also for 1 h. Studies of the coatings thus prepared revealed a small loss of hydrophobicity after long-term operation of the films containing TiO_2 (2 mass %); these films also exhibited photocatalytical self-cleaning of the surface and high transparency (~90%) throughout the visible spectral region.

Recently, template methods of surface texturing have become popular.[13, 23, 25, 26, 39, 40] This makes it possible to prepare both surfaces covered with pillars and porous substrates with a regular system of grooves. The advantage of these methods is the possibility of controllable variation of not only the density, but also the size of grooves and pillars. Usually, the preparation of textured surfaces by these techniques involves a number of steps.[13] First, the substrate surface is covered with a photoresist layer. Then, a template is made on the photoresist surface using a contact lithographic mask/pattern prepared with a high-resolution printer or using an electron beam. The template is transferred to the substrate using chemical etching; the duration and regime of this procedure determine the height of pillars or the depth of grooves on the final texture. The texture is made hydrophobic by treatment with hydrophobic materials with low surface energy. In particular, the surface of a textured silicon wafer was coated (by adsorption from vapour phase) with methylated or fluorinated organosilane layers.[13] The advancing contact angles on such surfaces were as large as 176°; however, a large hysteresis was observed, which strongly depended on the shape of the cross-section of pillars (Table 3). A drawback of photolithographic techniques is that this is applicable only to small surface areas. In addition, textures with pillars are mechanically unstable, which also reduces the field of application. Structures with grooves are mechanically more stable but inappropriate for attainment of the superhydrophobic state.

Table 3. Contact angles on surfaces textured using variously shaped pillars of height 40 μm and hydrophobised with dichlorodimethylsilane.[13]

Pillar shape and arrangement	Texture parameters	Contact angle /deg	
		advancing	receding
	staggered rhombus pillars, x = 8 μm	176	156
	star-like pillars, x = 8 μm	175	149
	indented square pillars, x = 8 μm	175	143
	square pillars,		
	x = 16 μm	173	134
	x = 23 μm	175	146
	x = 32 μm	173	154
	x = 56 μm	121	67

Template methods are widely used in nanotechnologies, but template-based design of superhydrophobic surfaces of materials is in the early stage of its development. For instance, bimodal roughness on glass substrates was formed using the template technique.[72] A monolayer of spherical polystyrene latex beads 5 μm in diameter used as the template was suspension coated on the substrate by spin coating. The monolayer was impregnated with a silver acetate (AgOAc) solution by capillary forces and a thin AgOAc layer was formed after subsequent drying of the lower surface of the

latex particles. Subsequent slow heating at 360 °C for 3 h led to thermal decomposition of AgOAc and formation of silver nanoparticles and their sintering, the template being removed simultaneously. The structure thus fabricated (Fig. 14) has a bimodal roughness with the characteristic size of silver nanoparticles of 150 nm (mean size) and 5 μm. The water contact angle on this textured surface reached a value of 169° after coating with a hexadecanethiol monolayer.

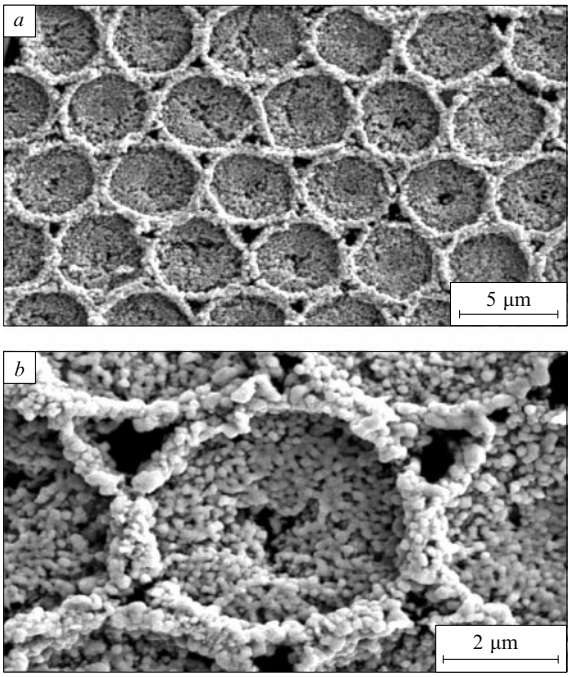


Figure 14. SEM images of a film made of silver nanoparticles with bimodal roughness at different magnification.[72]

Now we will consider in more detail a widely used method of preparation of superhydrophobic coatings that involves the use of organic and inorganic fillers with multimodal particle size distributions,[42–44, 66–71] such as silica,[44, 67] glass beads,[47] fluoride latexes,[66, 69] polystyrene latexes and carbon nanotubes.[68] On the surface of substrates, these particles either self-assemble to form a monolayer or aggregate with the formation of bimodal or multimodal roughness after evaporation of the dispersion medium. In particular, silica particles with sizes of 700 and 70 nm were used.[67] Large particles were coated with a film containing epoxy groups, while the smaller particles, with amino groups. The reaction between epoxy and amino groups led to covalent bonding of the small particles to the surface of the large ones. The composite particles thus prepared were deposited from dispersion in ethanol on an aluminium substrate coated with a film containing epoxy groups; this led to formation of bimodal roughness. The reaction between non-consumed amino groups on the surface of the small particles with the composite particles led to covalent binding of the latter to the surface of the epoxy coating of the substrate. Subsequent curing of the epoxy film resulted in embedding ot the particles into the epoxy matrix; binding to the surface of the monoepoxy-functionalised polydimethylsiloxane ensured the hydrophobic properties of the texture prepared.

Silica particles of primary diameter 16 nm were also used.[44] Deposition of these particles from dispersion in hexane in the presence of dichlorodimethylsilane on the surface of a glass substrate was followed by their aggregation. The shape of aggregates strongly depended on the structure of the substrate. For instance, an islet-shoped film made of aggregated particles was formed on a smooth surface, while the deposition after preliminary polishing of the surface gave a uniform distribution of the aggregated particles across the substrate surface with two characteristic roughness intervals, 0.2–1 μm and 40–80 nm. To impart hydrophobic properties to the texture thus prepared, its surface was coated with a polymeric film of a commercial hydrophobising reagent FC735 (blend of a fluoroacrylate polymer and fluoroalkyl ethers). It should be noted that the superhydrophobic state of the substrate was attained only in the case of uniform distribution of the aggregated particles across the substrate surface; the advancing contact angle was 170° and hysteresis was at most 2°.

The promise of the methods of preparation of superhydrophobic coatings based on the use of organic and inorganic fillers with multimodal particle size distribution is first of all due to the relative technological simplicity of coating of large surface areas. In addition, one can use composites; this makes it possible not only to impart hydrophobic properties to the surface of the texture, but also to chemically bind it to the substrate surface, which makes the hydrophobic coating more stable under the operating conditions.

Summing up, emphasise again that the key requirements for textures used to attain the superhydrophobic state of surfaces of materials include the maintenance of multimodal roughness of the surface and mechanical strength of the texture.

V. Coating of smooth and textured surfaces with hydrophobic agents

Numerous experiments showed that the surface energy and wettability depend not only on the chemical structure and texture of the surface. The contact angle also strongly depends on the orientation of molecules on the surface and on the degree of their ordering. The hydrophobising monolayers are most often coated using dip coating, spin coating, adsorption from solutions or from the vapour phase and the evaporating drop techniques.

The dip coating (or dipping) technique involves immersion of a substrate into, and subsequent removal from, a solution containing a hydrophobising reagent or a dispersion of hydrophobic particles. In the case of solution coating, the possibility of preparing coating with uniform thickness is governed by the possibility of immersing and removing the substrate at a constant velocity, whereas the thickness of the coating depends on the velocity of the motion of the receding (advancing) meniscus of the liquid, the concentration of hydrophobising reagents and the viscosity of the solution.[79–81] In addition, the diameter of particles is important when using dispersion coating.[82] Finally, the quality and structure of the coating are to a great extent determined by the character of the interaction of the hydrophobising components (hydrophobised particles of the dispersion) with the substrate, the solvent and with one another.

In the case of spin coating or centrifugation of a drop of a solution (or dispersion) on a rotating substrate, the possibility of prepareing coating with uniform thickness strongly depends on the rotation frequency and viscosity of the solution. In addition, an important role is played by the volatility of the solvent (dispersion medium), which determines both the equi-

librium character of the coating structure and its homogeneity with respect to thickness and the chemical composition.[80, 81]

Adsorption from solutions or vapour phase is mainly used for preparation of monolayered hydrophobic coatings based on, *e.g.*, self-assembled monolayers. Specific features and problems that arise when using this technique have been discussed in literature;[83–89] therefore, we will not dwell on them. We only point that the quality of the coating, its spatial homogeneity and roughness of the coated substrate depend to a great extent on the solvent used and the presence of water in the solvent, on the surface and in the surrounding atmosphere, as well as the temperature and pretreatment of the substrate surface. The contact angle attainable on a particular surface upon adsorption of a hydrophobising monolayer strongly depends on the density and regularity of the packing of the monolayer. Usually, self-assembled monolayers have many structural defects that deteriorate the hydrophobic properties. A method of preparation of mechanically assembled monolayers on relatively smooth surfaces, for which the contact angle reached a value of 130°, was proposed.[87] Figure 15 schematically shows the necessary process steps. A polydimethylsiloxane (PDMS) substrate (*1*) is pre-stretched (*2*) and exposed to ozone and UV irradiation to produce surface hydroxyl groups (*3*). In the next step (*4*) the surface is coated with a self-assembling chlorosilane monolayer by adsorption from the vapour phase. After stress relief, a closely packed monolayer of grafted molecules is formed on the substrate (*5*); the number of structural defects in the monolayer is much smaller than in the self-assembled monolayer on the non-pretreated substrate. The coating thus prepared is characterised by the largest contact contact angle for smooth surfaces.

The evaporating droplet technique is the fastest and simplest. It can be used for rough assessment of the properties of coatings. A drop of a solution (dispersion) containing a hydrophobising reagent is placed on the surface of a substrate where it spontaneously spills over. Films thus prepared usually have different thickness at different points and inhomogeneous chemical composition even if the substrate is completely wetted by the solution or dispersion. Similarly to the methods mentioned above, here the properties of the coating depend on the state of the surface, the solvent used, the temperature and humidity. Nevertheless, in some cases simplicity of the technique plays the determining role, because it allows the chemical composition, solvent, temperature, *etc.* to be chosen with ease in the design of novel coatings.[45]

Coatings prepared by the methods considered above usually differ not only in thickness, but also in the degree of ordering and orientation of molecules. This in turn affects the value of Young contact angle. For instance, for a gold substrate coated with alkanethiols by adsorption from solutions, the contact angle on the surface of the coating can be as large as 115–116°, being only 100–110° when using the dip coating technique. The contact angles on fluorinated chlorosilane monolayers coated using different techniques also vary from 100 to 114°. Here, the problem of choice of the method for applying hydrophobic coatings to attain the superhydrophobic state arises naturally. Analysis of experimental data on the contact angles on hydrophobised textured substrates showed that small variations of the Young angle do not preclude the obtaining of the effective contact angles larger than 150° on textures with multimodal roughness. However, obtaining small sliding angles for drops on such hydrophobic surfaces in each particular case requires thorough choice of the coating technique that provides the chemical and structural homogeneity of the coating. Yet another prerequisite for hydrophobic coatings is their chemical stability and wear resistance, because it is these properties that are responsible for long operating life of the coatings.

VI. Ageing and degradation of superhydrophobic coatings

The ability of hydrophobic and superhydrophobic materials to retain hydrophobic properties under operating conditions is of paramount importance when assessing potential fields of their application. Clearly, the ageing and degradation (loss of hydrophobic properties) are governed by both the properties of the coating and specific features of the operating conditions and the character of its interaction with the environment. Unfortunately, the problem of durability of hydrophobic materials has not been cosidered in detail in the literature. In this Section we will briefly outline a number of studies on the subject.

When materials are used in air, the loss of hydrophobic properties is due to atmospheric pollution. Usually, surfaces become significantly more hydrophilic upon deposition of dust and organic chemicals. To reduce this effect, it was proposed [62] to add titania to the hydrophobising coatings for glass elements of buildings. Titania possesses photocatalytic activity and organic residues exposed to UV radiation in the presence of TiO_2 are oxidised to CO_2. Outdoor exposure tests of coatings with different content of titania were carried out in Tokyo (Japan) in winter at a height of 20 m from the ground level. The tests showed that degradation of the coatings caused by stains occurs much more slowly in the presence of small amounts of TiO_2 (~2 mass %) and faster in the presence of

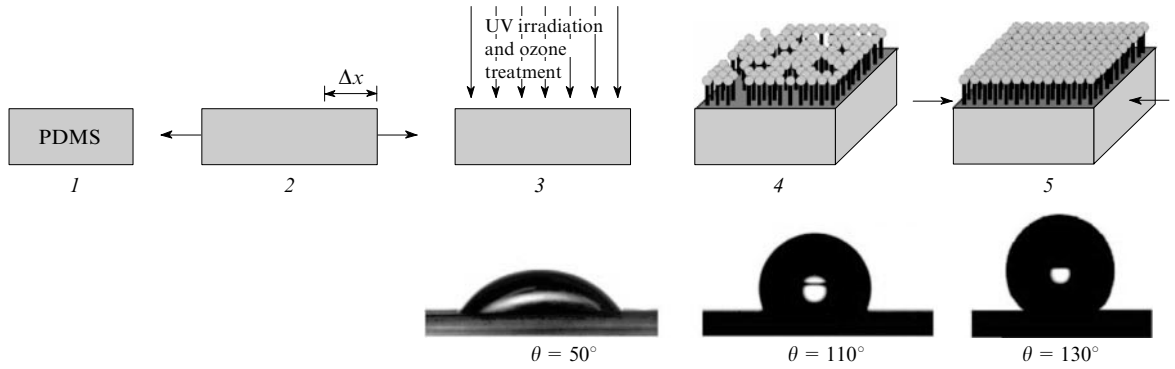


Figure 15. Process steps leading to production of mechanically assembled monolayer.[87] For notations (*1–5*), see text.

larger content of titania (Fig. 16). At the optimal concentration of TiO_2, the water contact angle decreased from 150 to 140° after 75 days (*cf.* the range from 148° to 100° for the hydrophobic coating with no TiO_2 additives).

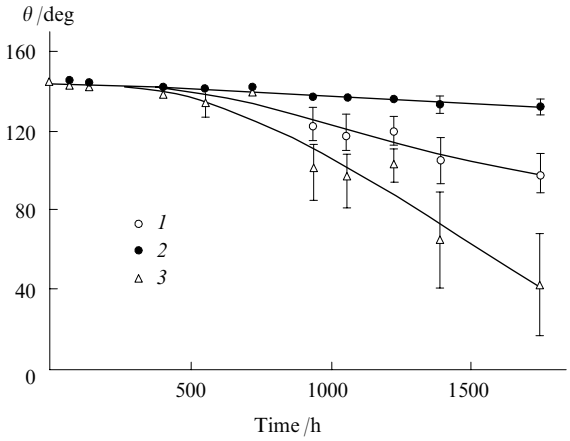


Figure 16. Changes in contact angle on the surface coated with a composite alumina/titania hydrophobising film plotted *vs.* film exposure time under atmospheric conditions.[62]
TiO_2 content /mass %: 0 (*1*), 2 (*2*) and 20 (*3*).

The problem of ageing of hydrophobic coatings was also considered in another study.[89] The surface of a sample was hydrophobised by keeping of the sample in carbon tetrafluoride plasma. Two types of samples were studied, (i) PDMS containing no fillers (they were removed by centrifugation) and (ii) PDMS filled with large amount of quartz. Keeping in plasma led to hydrophobisation of the surface due to fluorination and to simultaneous enhancement of roughness. At residence times of no longer than 15 min, a layer containing C_mF_n ($m > 1$) or CF_xH_{3-x} ($0 < x < 3$) groups was formed on the PDMS surface and the surface energy considerably decreased. Ageing of this surface in air was studied by elemental analysis (Table 4). In particular, it was found that on long-term treatment of samples the content of carbon and oxygen increased, that of fluorine decreased, whereas the amount of silicon remained virtually unchanged. After keeping in air for 5 weeks, the atomic concentration of fluorine was 93% with respect to the initial concentration in the samples with the filler and 89% in the samples with no filler. The smaller loss of hydrophobicity of the Teflon-like surface with quartz filler was explained by rigid binding of fluorosilane groups to the filler surface.

Table 4. Elemental composition (in %) of the surface of etched polydimethylsiloxane sample (CF_4 plasma, etching duration 15 min) cured in air.[89]

Curing duration	PDMS with quartz filler				PDMS with no filler			
	C	Si	O	F	C	Si	O	F
Freshly prepared sample	18.7	5.8	10.8	64.7	18.9	4.8	18.8	57.5
5 days	19.7	5.9	11.2	63.2	21.2	5.2	19.5	54.2
15 days	19.3	6.5	12.0	62.2	22.4	5.3	19.6	52.7
35 days	20.9	6.4	12.4	60.3	23.7	5.3	20.1	50.9

Ageing of superhydrophobic anticorrosion coatings with different compositions on the carbon steel surface was studied.[66] The surface of a steel sample was coated with either a layer of Ni–P composite or a phosphate film with complex chemical composition to provide corrosion resistance and specify the topography. Then the dip coating technique was used to coat the corrosion resistant layer with a solution of a hydrophobising reagent that contained a fluoride latex and the system was heated at 150–200 °C for 1–2 h. The contact angles on the freshly prepared coatings based on the phosphate film were in the interval 155–168° and changed only slightly on storage under laboratory conditions. For instance, the contact angle on these films decreased by ~3° after 45 days, while the sliding angle considerably increased from 2–3 to 15–20°. Storage of the coatings in water led to a decrease in the contact angle by 4° after 24 h and by 6° after 48 h. The sliding angle increased by 2° after 48 h. The results of water erosion test and the character of the interaction of the samples with 0.5% NaCl solution showed that the coatings with superhydrophobic surface layer exhibited much better corrosion resistance compared to the coatings having no hydrophobic layer.

Superhydrophobic surfaces with multimodal roughness (Fig. 17) can be prepared by coating various materials with a textured system based on silica nanoparticles treated with

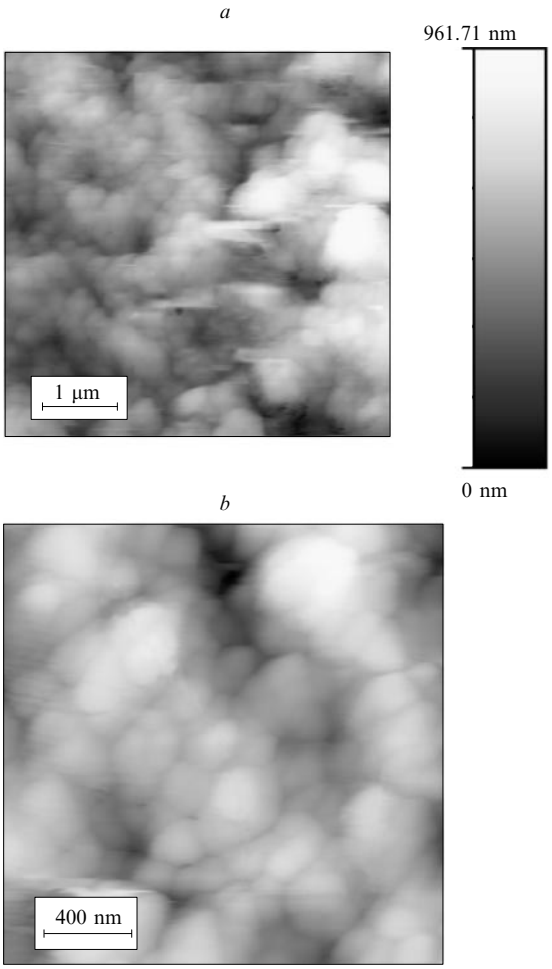


Figure 17. AFM images of the a surface of superhydrophobic coating prepared by deposition of dispersed aerosil on a silicon latex substrate followed by hydrophobisation with fluoroxyaminosilanes obtained at different magnification.[45]

fluoroxyaminosilanes. Tests for retention of superhydrophobic properties of these coatings revealed a decrease in the contact angle from 158 to 156° after storage under atmospheric conditions for 60 days, while the sliding angle of the drop remained unchanged (~5°). The results of investigations of the dynamics of hydrophobicity loss on long-term contact with water suggest that the coating prepared provides contact angles that are larger than 150° and completely protects the surface from water for 10–15 h. However, the hydrophobic properties of the surface are little changed even on longer time of contact with water. For instance, the contact angle on the coating decreased by 18° over a period of 48 h. Tests of the same coatings in salt, weakly acidic and weakly alkaline solutions revealed slight changes in the degree of hydrophobicity over a period of 2–4 h of continuous contact with the solution (Fig. 18).

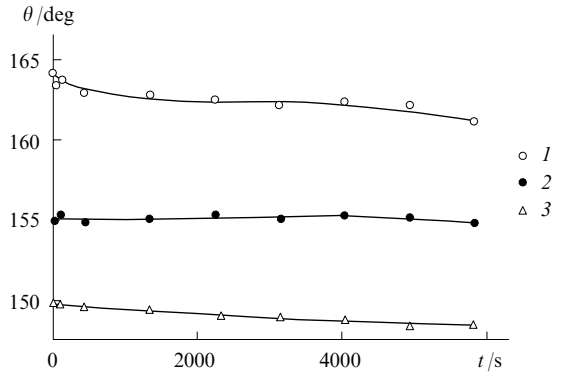


Figure 18. Dynamics of changes in the contact angle of aqueous solution droplets on the surface covered with a textured superhydrophobic coating.[45]
Alkaline solution with pH 7.45 (*1*), 0.5 M solution NaCl (*2*) acid solution with pH 6 (*3*).

It should be noted that on prolonged contact the hydrophobic coating reacts with water the degree of the reaction being dependent on the chemical structure of the hydrophobising reagent. Therefore, a prerequisite for extension of the durability of a hydrophobic coating is minimisation of the surface area of the contact with the liquid. This can be attained in the case of heterogeneous wetting.

VII. Applications of highly hydrophobic and superhydrophobic materials and coatings

Hydrophobic materials are widely used at present. Now we will give a few examples of the use of materials the hydrophobic and superhydrophobic properties of which are attained by choosing the chemical composition of the surface and specific texturing.

Treatment of the surface of satellite antennas with superhydrophobic coatings developed by researchers at NTT (Japan) led to significant reduction of the adhesion of snow to metallic antenna surfaces[89] and, as a consequence, the number of satellite communications' breakdown events decreased.

An efficient device for separation of aqueous and oil phases was made using tailored textured coatings on microsieves[90] The operation of such sieves is based on the use of strongly different contact angles of water and oil on the surface of the sieve. For instance, the advancing contact angle of water is larger than 156° and the sliding angle of water is ~4°. At the same time the surface remained oleophilic. Water–oil emulsion in this sieve was rapidly separated, because oil droplets passed through the openings in the sieve to the lower tank.

Textile fibres with nanostructured surface are suitable for production of hydrophobic cloth based on cotton fibres[91] and manufacturing of self-cleaning ties and shirts (no wash is required).[92]

The use of superhydrophobic coatings in electrical engineering appeared to be highly efficient. For instance, coating conductors of power lines with superhydrophobic films considerably reduced the noise due to corona discharges produced by water drops on the surface of conductors.[93]

We have developed hydrophobic coatings with multimodal roughness for the surface of silicon insulators for high-voltage power lines. This makes it possible to significantly reduce the intensity of the interaction of the material of the insulator with atmospheric precipitates and, therefore, to reduce the leakage currents flowing across the surface of the insulators.[45]

Now we will dwell on the use of textured hydrophobic materials as adaptive materials that can change their properties under the action of external factors. The chemical properties and wetting of such materials can vary upon irradiation,[94–96] in an electric field,[97–99] on heat treatment,[100] treatment with solutions[61, 101] and as a result of change in the pH value.[64]

Reversible changes in the wetting properties of surfaces from superhydrophobicity to superhydrophilicity (Fig. 19) on exposure to UV radiation were observed for zinc,[55, 103–105] titanium,[106–108] tin[109] and tungsten[110] oxides. They were used by researchers from PPG Industries (USA) and Pilkington (UK) for fabrication of self-cleaning glasses. There are two mechanisms of self-cleaning. In the daytime, exposure to UV

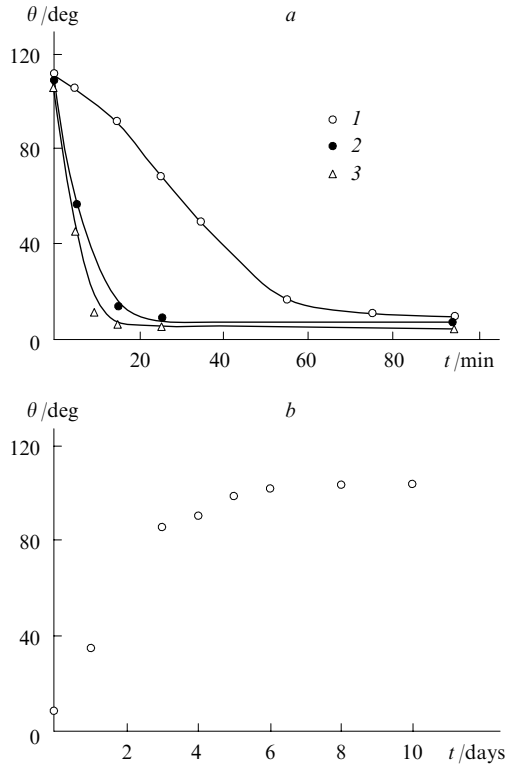


Figure 19. Time dependences of contact angle of ZnO surface exposed to UV radiation with a light intensity of 0.1 (*1*), 2.0 (*2*) and 50 mW cm^{-2} (*3*) (*a*) and on storage of the irradiated samples in the dark (*b*).[102]

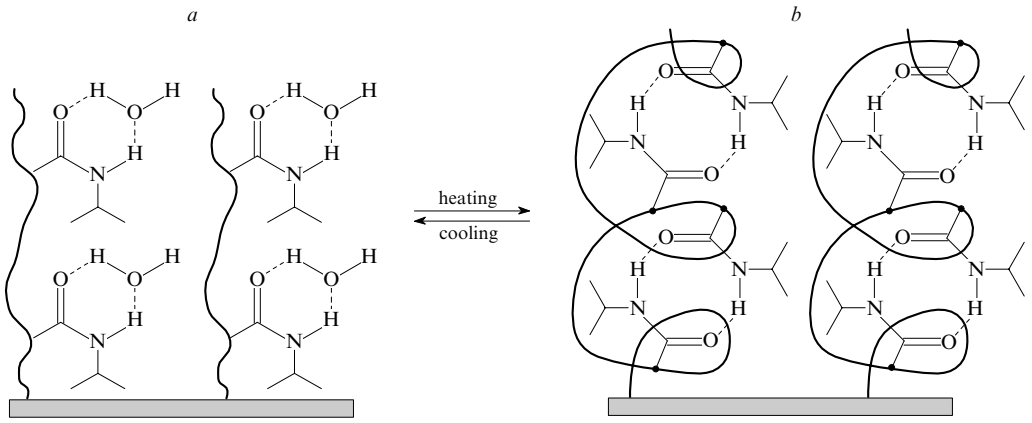


Figure 20. Reversible conformational transition with formation of stretched (*a*) and helical (*b*) conformations of poly(*N*-isopropylacetamide) chains on heating and cooling.

radiation causes (i) photocatalytic decomposition of organic and (ii) hydrophilisation of the surface due to additional adsorption of water molecules initiated by radiation. Stains are washed out from such surfaces either by rain or by artificial irrigation. Storage of the surface in the dark for some time recovers the superhydrophobic state and the second mechanism operates; it is associated with absorption of stains having weak adhesion to glass by water drops sliding across the superhydrophobic surface. Here, the contact angle decreased on exposure to UV radiation from 109 to 10° on smooth ZnO surface and from 163 to 0° on the textured surface.

Photoswitchable wetting has found an interesting application in microfluidics and in organic synthesis. Namely, a macroscopic motion of small liquid droplets across a photosensitive surface used for the delivery of components to the reaction zone can be driven by irradiation.[94] A monolayer based on azobenzene derivatives made the surface photosensitive. UV irradiation of the surface at $\lambda = 360$ nm caused photoisomerisation with an increase in the proportion of *cis*-isomers, which impart the hydrophilic properties to the surface. Irradiation with blue light at $\lambda = 436$ nm caused *cis*–*trans*-isomerisation and the surface returned to the hydrophobic state. If a droplet a few millimetres in size is placed on such a surface and asymmetrical (with respect to the wavelength) illumination is created, the surface energy difference between different points along the perimeter is sufficient for the droplet to move. This motion can be controlled with high accuracy.

Yet another application of photoswitchable wetting was proposed.[111] The surface of nanoporous aluminium membranes was modified with a mixture of spiropyran and hydrophobic molecules. A non-illuminated membrane contained the non-polar form of spiropyran, which ensured nonwetting of the membrane by aqueous solutions. On UV irradiation, spiropyran undergoes transition to the polar merocyanine form and the water molecules and dissolved ions can pass across the membrane. Thus, the membrane operates as a photosensitive valve, which switches the water and ion transport and changes the ionic conductivity.

Temperature-switchable wetting observed in a number of systems characterised by the lower critical solution temperature can be employed to preclude biofouling of surfaces. The best studied polymer possessing this property is poly(*N*-isopropylacetamide) (PNIPAAm). The wetting transition is associated with conformational changes in the PNIPAAm molecules grafted to the surface (Fig. 20). It was shown[100] that this conformational transition on heating causes contact angle on the PNIPAAm-coated surface to change from 63 to 93°. By texturing the surface with micrometre-size grooves, it is possible to induce the transition from superhydrophobicity to superhydrophilicity with very small wetting hysteresis. The system is characterised by multiple cycling of the wetting regimes without degradation of coatings (Fig. 21).

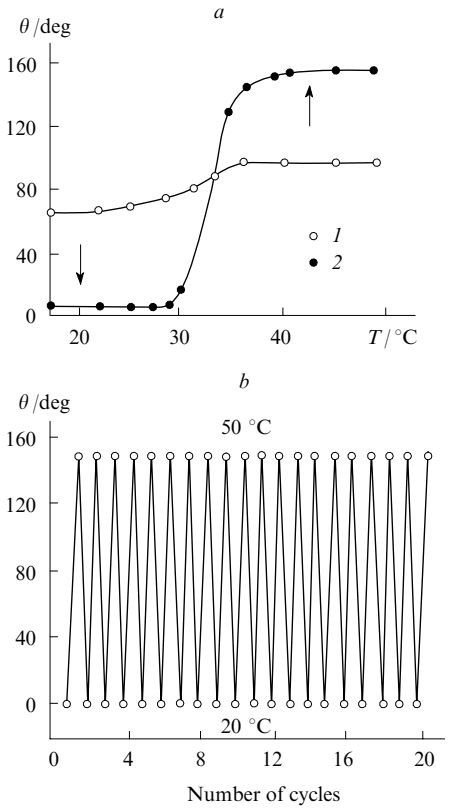


Figure 21. Temperature dependence of the water contact angle on PNIPAAm film (*a*) and cyclic switching between wetting regimes on a textured surface on heating and cooling (*b*).[100]
Smooth surface (*1*) and textured surface with micrometre-size grooves (*2*). Arrows denote the directions of changes in the angle θ due to surface texturing.

VIII. Conclusion

In this review, we considered the key principles of the design of highly hydrophobic and superhydrophobic materials and coatings. The design of such materials implies the use of low-energy coatings along with surface texturing characterised by multimodal roughness. A prerequisite that ensures the superhydrophobic properties of a material is the surface texturing in such a manner that heterogeneous wetting of the surface be thermodynamically stable. Meeting this condition allows a number of technological problems to be solved at once. First of all, this makes it possible to reduce wetting hysteresis and, therefore, to ensure self-cleaning properties of the hydrophobic surface because water drops sliding from the surface carry away waste characterised by low adhesion towards the material. In addition, in this regime the surface area of the contact between the coating material and the liquid is minimal and therefore degradation of the hydrophobic state as a result of the reaction with water occurs more slowly.

We believe that even the short list of studies on methods of preparation of textured hydrophobic surfaces of different nature cited in this review and a few examples of application of highly hydrophobic and superhydrophobic materials provide a clear idea of a great potential of this field of materials science.

However, a number of problems to be solved should also be mentioned. The key factors that limit the use of hydrophobic materials are insufficiently high wear resistance and chemical instability of the hydrophobic layers. In some cases, the surface texture and coatings that ensure optimum hydrophobic properties of the surface are characterised by insufficiently high mechanical strength. Of particular importance for long-term durability of hydrophobic materials is the development of methods for surface cleaning from organic waste that pollute the surface of materials under atmospheric conditions. Slowing down degradation of hydrophobic state due to the reaction with water in the case of underwater and underground operation of hydrophobic materials is still topical. It seems likely that major efforts of researchers and materials scientists who work in the field of design of hydrophobic and superhydrophobic materials and coatings will be focused on solving these problems in the nearest future.

The review is based on the results of studies carried out by the authors with the financial support from the Russian Foundation for Basic Research (Project No. 08-08-12130) and the State Programme for Support of Leading Scientific Schools (under Contract No. 02.516.11.6081).

References

1. T Young *Philos. Trans. R. Soc. London* **95** 65 (1805)
2. A A Thorpe, V Peters, J R Smith, T G Nevell, J Tsibouklis *J. Fluorine Chem.* **104** 37 (2000)
3. W Chen, A Fadeev, M Hsieh, D Oner, J Youngblood, T J McCarthy *Langmuir* **15** 3395 (1999)
4. J Genzer, K Efimenko *Biofouling* **22** 339 (2006)
5. T Nishino, M Meguri, K Nakamae, M Matsushita, Y Ueda *Langmuir* **15** 4321 (1999)
6. B V Derjaguin, N V Churaev, V M Muller *Poverkhnostnye Sily* (Surface Forces) (Moscow: Nauka, 1985)
7. N V Churaev *Kolloid. Zh.* **65** 293 (2003) [a]
8. L B Boinovich, A M Emelyanenko *Izv. Akad. Nauk, Ser. Khim.* 256 (2008) [b]
9. L B Boinovich *Usp. Khim.* **76** 510 (2007) [*Russ. Chem. Rev.* **76** 471 (2007)]
10. I Woodward, W C E Schofield, V Roucoules, J P S Badyal *Langmuir* **19** 3432 (2003)
11. A Tserepi, E Gogolides, K Tsougeni, V Constantoudis, E Valamontes *J. Appl. Phys.* **98** 113502 (2005)
12. Y Zhao, Q Lu, D Chen, Y Wei *J. Mater. Chem.* **16** 4504 (2006)
13. D Oner, T J McCarthy *Langmuir* **16** 7777 (2000)
14. A B D Cassie *Discuss. Faraday Soc.* **3** 11 (1948)
15. P S Swain, R Lipowsky *Langmuir* **14** 6772 (1998)
16. A B D Cassie, S Baxter *Trans. Faraday Soc.* **40** 546 (1944)
17. A M Emelyanenko, L B Boinovich, in *The 13th International Conference on Surface Forces (Book of Abstracts), Moscow, 2006* p. 43
18. R Wenzel *Ind. Eng. Chem.* **28** 988 (1936)
19. B V Derjaguin *Dokl. Akad. Nauk SSSR* **51** 357 (1946) [c]
20. A Marmur *Langmuir* **19** 8343 (2003)
21. A Marmur *Langmuir* **20** 3517 (2004)
22. N A Patankar *Langmuir* **19** 1249 (2003)
23. B He, N A Patankar, J Lee *Langmuir* **19** 4999 (2003)
24. O Werner, L Wagberg, T Lindstrom *Langmuir* **21** 12235 (2005)
25. L Barbieri, E Wagner, P Hoffman *Langmuir* **23** 1723 (2007)
26. J Bico, C Marzolin, D Quere *Europhys. Lett.* **47** 220 (1999)
27. E Bormashenko, R Pogreb, G Whyman, M Erlich *Langmuir* **23** 6501 (2007)
28. S Daniel, S Sircar, J Gliem, M K Chaudhury *Langmuir* **20** 4085 (2004)
29. D Quere, A Lafuma, J Bico *Nanotechnology* **14** 1109 (2003)
30. L Feng, Y Song, J Zhai, B Liu, J Xu, L Jiang, D Zhu *Angew. Chem., Int. Ed.* **42** 800 (2003)
31. T Sun, L Feng, X Gao, L Jiang *Acc. Chem. Res.* **38** 644 (2005)
32. M E Abdelsalam, P N Bartlett, T Kelf, J Baumberg *Langmuir* **21** 1753 (2005)
33. A Tuteja, W Choi, M Ma, J M Mabry, S A Mazzella, G C Rutledge, G H McKinley, R E Cohen *Science* **318** 1618 (2007)
34. A Lafuma, D Quere *Nat. Mater.* **2** 457 (2003)
35. K Wier, T J McCarthy *Langmuir* **22** 2433 (2006)
36. C Dorrer, J Ruhe *Langmuir* **23** 3820 (2007)
37. A Marmur *Langmuir* **22** 1400 (2006)
38. Z Yoshimitsu, A Nakajima, T Watanabe, K Hashimoto *Langmuir* **18** 5818 (2002)
39. E Martines, K Seunarine, H Morgan, N Gadegaard, C D W Wilkinson, M Riehle *Nano Lett.* **5** 2097 (2005)
40. E Martines, K Seunarine, H Morgan, N Gadegaard, C D W Wilkinson, M Riehle *Langmuir* **22** 11230 (2006)
41. J Y Shiu, C W Kuo, P Chen, C Y Mou *Chem. Mater.* **16** 561 (2004)
42. M Hikita, K Tanaka, T Nakamura, T Kajiyama, A Takahara *Langmuir* **21** 7299 (2005)
43. G Zhang, D Wang, Z-Z Gu, H Mohwald *Langmuir* **21** 9143 (2005)
44. M Ferrari, F Ravera, L Liggieri *Appl. Phys. Lett.* **88** 203125 (2006)
45. L B Boinovich, A M Emelyanenko, A M Muzafarov, A M Myshkovskii, A S Pashinin, A Yu Tsivadze, D I Yarova *Ross. Nanotekhnol.* **3** (9–10) (2008) [d]
46. Y T Cheng, D E Rodak, C A Wong, C A Hayden *Nanotechnology* **17** 1359 (2006)
47. R H Dettre, R R Johnson Jr, in *Contact Angle, Wettability and Adhesion (Advances in Chemistry Series)* (Washington DC: American Chemical Society, 1963) Vol. 43, p. 136
48. D Quere *Rep. Prog. Phys.* **68** 2495 (2005)
49. F E Bartell, J W Sheppard *J. Phys. Chem.* **57** 211 (1953)
50. S Shibuichi, T Onda, N Satoh, K Tsujii *J. Phys. Chem.* **100** 19512 (1996)
51. T Onda, S Shibuichi, N Satoh, K Tsujii *Langmuir* **12** 2125 (1996)
52. H Y Erbil, A L Demirel, Y Avci, O Mert *Science* **299** 1377 (2003)
53. N R Chiou, C Lu, J Guan, L J Lee, A J Epstein *Nat. Nanotechnol.* **2** 354 (2007)
54. K K S Liu, J Bico, K K B Teo, M Chhowalla, G A J Amaratunga, W I Milne, G H McKinley, K K Gleason *Nano Lett.* **3** 1701 (2003)

55. H Liu, L Feng, J Zhai, L Jiang, D Zhu *Langmuir* **20** 5659 (2004)
56. Z Wang, L Ci, L Chen, S Nayak, P M Ajayan, N Koratkar *Nano Lett*. **7** 697 (2007)
57. S Li, H Li X Wang, Y Song, Y Liu, J Zhai, L Jiang, D Zhu *J. Phys. Chem. B* **106** 9274 (2002)
58. H Liu, S Li, J Zhai, H Li Q Zheng, Y Song, L Jiang, D Zhu *Angew. Chem., Int. Ed.* **43** 1146 (2004)
59. M Lejeune, L M Lacroix, F Bretagnol, A Valsesia, P Colpo, F Rossi *Langmuir* **22** 3057 (2006)
60. K Tsougeni, A Tserepi, G Boulousis, V Constantoudis, E Gogolides *Jpn. J. Appl. Phys. Part 1* **46** 744 (2007)
61. S Minko, M Muller, M Motornov, M Nitschke, K Grundke, M Stamm *J. Am. Chem. Soc*. **125** 3896 (2003)
62. A Nakajima, K Hashimoto, T Watanabe, K Takai, G Yamauchi, A Fujishima *Langmuir* **16** 7044 (2000)
63. A Nakajima, A Fujishima, K Hashimoto, T Watanabe *Adv. Mater*. **16** 1365 (1999)
64. Y Jiang, Z Wang, X Yu, F Shi, H Xu, X Zhang *Langmuir* **21** 1986 (2005)
65. M Li, J Zhai, H Liu, Y Song, Y Jiang, D Zhu *J. Phys. Chem. B* **107** 9954 (2005)
66. L Zhu, Y Jin *Appl. Surf. Sci*. **253** 3432 (2007)
67. W Ming, D Wu, R van Benthem, G de With *Nano Lett*. **5** 2298 (2005)
68. Y Li, X J Huang, S H Heo, C C Li, Y K Choi, W P Cai, S O Cho *Langmuir* **23** 2169 (2007)
69. A Tokuumi, K Hiromatsu, S Kumai, H Mihara *Tosu-to-Toryo* **571** 37 (1998)
70. J Bravo, L Zhai, Z Wu, R E Cohen, M F Rubner *Langmuir* **23** 7293 (2007)
71. P-S Tsai, Y-M Yang, Y-L Lee *Nanotechnology* **18** 1 (2007)
72. Y Li, C Li, S O Cho, G Duan, W Cai *Langmuir* **23** 9802 (2007)
73. L Zhang, Z Zhou, B Cheng, J M DeSimone, E T Samulski *Langmuir* **22** 8576 (2006)
74. M Sun, C Luo, L Xu, H Ji, Q Ouyang, D Yu, Y Chen *Langmuir* **21** 8978 (2005)
75. Z Yuan, H Chen, J Tang, H Gong, Y Liu, Z Wang, P Shi, J Zhang, X Chen *J. Phys. D* **40** 3485 (2007)
76. E Puukilainen, T Rasilainen, M Suvanto, T Pakkanen *Langmuir* **23** 7263 (2007)
77. B Qian, Z Shen *Langmuir* **21** 9007 (2005)
78. M F Wang, N Raghunathan, B Ziaie *Langmuir* **23** 2300 (2007)
79. B V Derjaguin, S M Levi *Fiziko-khimiya Naneseniya Tonkikh Sloev na Dvizhushchuyusya Podlozhku* (Physical Chemistry of Applying Thin Layers on Moving Substrates) (Moscow: Academy of Sciences of the USSR, 1959)
80. P Yimsiri, M R Mackley *Chem. Eng. Sci*. **61** 3496 (2006)
81. E J Nassar, K J Ciuffi, R R Goncalves, Y Messaddeq, S J L Ribeiro *Quim. Nova* **26** 674 (2003)
82. M Ghosh, F Fan, K J Stebe *Langmuir* **23** 2180 (2007)
83. A Ulman *An Introduction to the Ultrathin Organic Films from Langmuir-Blodgett to Self-Assembly* (San Diego, CA: Academic Press, 1991)
84. A Ulman *Chem. Rev*. **96** 1553 (1996)
85. R D Peters, P F Nealey, J N Crain, F J Himpsel *Langmuir* **18** 1250 (2002)
86. M Wang, K M Liechti, Q Wang, J M White *Langmuir* **21** 1848 (2002)
87. J Genzer, K Efimenko *Science* **290** 2130 (2000)
88. Y H Yan, M B Chan-Park, C Y Yue *Langmuir* **21** 8905 (2005)
89. A Nakajima, T Watanabe, K Hashimoto *Monatsh. Chem*. **132** 31 (2001)
90. L Feng, Z Zhang, Y Mai, Y Ma, B Liu, L Jiang, D Zhu *Angew. Chem., Int. Ed*. **43** 2012 (2004)
91. T Wang, X Hu, S Dong *Chem. Commun*. 1849 (2007)
92. D Cyranoski *Nature (London)* **414** 240 (2001)
93. K Miyajima, K Tanabe *Technical Report of IEICE, EMCJ2000-51, 2000* p. 65
94. K Ichimura, S K Oh, M Nakagawa *Science* **288** 1624 (2000)
95. A Athanassiou, M I Lygeraki, D Pisignano, K Lakiotaki, M Varda, E Mele, C Fotakis, R Cingolani, S H Anastasiadis *Langmuir* **22** 2329 (2006)
96. S Wang, Y Song, L Jiang *J. Photochem. Photobiol. C: Photochem. Rev*. **8** 18 (2007)
97. J Lahann, S Mitragotri, T Tran, H Kaido, J Sundaram, I S Choi, S Hoffer, G A Somorjai, R A Langer *Science* **299** 371 (2003)
98. M Vallet, M Vallade, B Berge *Eur. Phys. J. B* **11** 583 (1999)
99. T N Krupenkin, J A Taylor, T M Schneider, S Yang *Langmuir* **20** 3824 (2004)
100. T Sun, G Wang, L Feng, B Liu, Y Ma, L Jiang, D Zhu *Angew. Chem., Int. Ed*. **43** 357 (2004)
101. Y Zhu, M Shi, J Xi, X Wu *Acta Chim. Sinica* **65** 1487 (2007)
102. R D Sun, A Nakajima, A Fujishima, T Watanabe, K Hashimoto *J. Phys. Chem. B* **105** 1984 (2001)
103. X Feng, J Zhai, L Jiang *J. Am. Chem. Soc*. **126** 62 (2004)
104. X Q Meng, D X Zhao, J Y Zhang, D Z Shen, Y M Lu, L Dong, Z Y Xiao, Y C Liu, X W Fan *Chem. Phys. Lett*. **413** 450 (2005)
105. X T Zhang, S Sato, A Fujishima *Langmuir* **20** 6065 (2004)
106. H Irie, T S Ping, T Shibata, K Hashimoto *Electrochem. Solid State Lett*. **8** D23 (2005)
107. X Feng, J Zhai, L Jiang *Angew. Chem., Int. Ed*. **44** 5115 (2005)
108. X Zhang, M Jin, Z Liu, D A Tryk, S Nishimoto, T Murakami, A Fujishima *J. Phys. Chem. C* **111** 14521 (2007)
109. W Zhu, X Feng, L Feng, L Jiang *Chem. Commun*. 2753 (2006)
110. S Wang, X Feng, J Yao, L Jiang *Angew. Chem., Int. Ed*. **45** 1264 (2006)
111. I Vlassiouk, C D Park, S A Vail, D Gust, S Smirnov *Nano Lett*. **6** 1013 (2006)

[a] — *Colloid J. (Engl. Transl.)*
[b] — *Russ. Chem. Bull., Int. Ed. (Engl. Transl.)*
[c] — *Dokl. Phys. Chem. (Engl. Transl.)*
[d] — *Nanotechnol. Russ. (Engl. Transl.)*